University of Tartu
Faculty of Science and Technology
Institute of Physics

Karl Ehatäht

Constraints on the mass and charge of millicharged dark matter

Bachelor's Thesis

Supervisors:
MSc Hardi Veermäe
PhD Luca Marzola

Tartu 2015

Contents

1. Introduction

Although the discovery of Higgs boson in 2013 completed one of the pillars of modern physics – the Standard Model (SM) – there are doubts that a new particle or particles must be introduced in order to agree with the astrophysical observations. These observations hint that about 26.8% of the Universe is made up of hypothetical kind of matter, called the Dark Matter (DM). Its gravitational effects on the visible sector suggest that DM has a weak interaction strength, but its general properties have still remained unknown.

One of the many DM candidates include millicharged particles (MCPs) – the particles which have a really tiny nonquantized electric charge compared to the quarks and leptons of SM. Any particle bearing an electric charge must interact with the photon. If these particles are charged under $U(1)$ gauge group, then by the symmetry requirement they also must have a corresponding antiparticle with the same charge of opposite sign. There exists many mechanisms where MCPs naturally arise from unified theories. The simplest way to treat MCPs would be considering them as new particles symmetric under $U(1)_{EM}$. More complex theories extend the gauge group of SM so that new gauge bosons mix with the photon, thus making „dark charge carriers" of the hidden sector visible through feeble electromagnetic interactions.

MCPs cannot have arbitrary charge and mass as these particles should affect the outcome of certain type of experiments and currently established models of cosmology. Since the existence of MCPs should agree with the experiments and observations, some bounds can be set on their properties.

The thesis focuses on a simplified theory of MCPs and tries to determine the relations between their mass and charge so that the model meets the limits set by the abundance of DM. It involves solving the Boltzmann equation for MCPs with the condition that their initial abundance is negligible after cosmic inflation. Particular emphasis lies on vector boson MCPs as their properties haven't been investigated yet within cosmology (except for theories that aren't very model-specific).

The outline of this thesis goes as follows: first a summary of the current state of constraints on the mass and charge of the MCPs is given; the calculation of the cross-section for the process $\gamma\gamma \to$ MCPs is carried out in the second chapter, which is then

used as an input to solve the Boltzmann equation and determine the bounds on their mass and charge in the third chapter. The second goal of this thesis is to get acquainted with the methods used in cosmology and quantum field theory. A minimal knowledge of quantum field theory, group theory and particle physics is expected from the reader.

All the numerical and intensive computations have been performed by using the *Mathematica* software. In the following we adopt natural units, for which $\hbar = c = G = k_B = 1$.

2. Known constraints on MCPs

This chapter is devoted to a brief review of the methods that have been used to bound the properties of millicharged scalar bosons and fermions.

It has been shown that MCPs can arise naturally from various unified theories which contain extra $U(1)_{\mathrm{MCP}}$ gauge degrees of freedom [1]. The gauge boson of this additional $U(1)$ group introduces a new field B_μ known as hidden, mirror or dark photon. New fermions, charged under $U(1)_{\mathrm{MCP}}$, obtain an electric charge, $q \equiv \epsilon e$, after diagonalization of the kinetic mixing term $-\frac{1}{2}\chi F^{\mu\nu}G_{\mu\nu}$, where $G_{\mu\nu} = \frac{1}{2}\partial_{[\mu}B_{\nu]}$ and χ is adimensional coupling [2]. To clarify the point, the Lagrangian in question reads (omitting the kinetic terms for the spinor fields) $\mathcal{L} = -\frac{1}{4}F^{\mu\nu}F_{\mu\nu} - \frac{1}{4}G_{\mu\nu}G^{\mu\nu} - \frac{1}{2}\chi F^{\mu\nu}G_{\mu\nu} + ej^e_\mu A^\mu + q'j^B_\mu B^\mu$, where q' and j^B_μ are $U(1)_{\mathrm{MCP}}$ charge and current, respectively. The kinetic mixing term is allowed because each field strength tensor is invariant under its own gauge group. The first three terms are recognized as quadratic form which can be cast into matrix form as follows:

$$\mathcal{L} = -\frac{1}{4}\begin{pmatrix} F_{\mu\nu} & G_{\mu\nu} \end{pmatrix}\begin{pmatrix} 1 & \chi \\ \chi & 1 \end{pmatrix}\begin{pmatrix} F^{\mu\nu} \\ G^{\mu\nu} \end{pmatrix} + ej^e_\mu A^\mu + q'j^B_\mu B^\mu\,.$$

In order to diagonalize the middle matrix one defines a new field $\widetilde{B}^\mu \equiv B^\mu + \chi A^\mu$, which in turn gives $G^{\mu\nu} = \partial^\mu B^\nu - \partial^\nu B^\mu = \partial^\mu(\widetilde{B}^\nu - \chi A^{nu}) - \partial^\nu(\widetilde{B}^\mu - \chi A^\mu) = \partial^\mu\widetilde{B}^\nu - \partial^\nu\widetilde{B}^\mu - \chi(\partial^\mu A^\nu - \partial^\nu A^\mu) \equiv \widetilde{G}^{\mu\nu} - \chi F^{\mu\nu}$. The Lagrangian remains unchanged after diagonalization,

$$\mathcal{L} = -\frac{1}{4}\begin{pmatrix} F_{\mu\nu} & \widetilde{G}_{\mu\nu} \end{pmatrix}\begin{pmatrix} 1-\chi^2 & 0 \\ 0 & 1 \end{pmatrix}\begin{pmatrix} F^{\mu\nu} \\ \widetilde{G}^{\mu\nu} \end{pmatrix} + ej^e_\mu A^\mu + q'j^B_\mu \widetilde{B}^\mu - \chi q'j^B_\mu A^\mu\,,$$

but from the last term it can be seen that the MCP current now couples to the visible photon with a coupling strength $-\chi q'$ which can be reinterpreted as the millicharge q. Thus this mechanism makes the „hidden" particles of a possible dark sector „visible" to our world through a millicharge.

The millicharged fermions can take up any fractional electric charge (while any other SM particle remains neutral under $U(1)_{\mathrm{MCP}}$). However, the constraints also involve their mass, m, and are usually given in the form $f(q, m) < const$, whereby f is not necessarily an analytic function.

2.1. Constraints from cosmology

Big Bang Nucleosynthesis

Big Bang Nucleosynthesis (BBN) refers to the production of light atom nuclei such as D, ^{3}He, ^{4}He and ^{7}Li. By that time the Universe had cooled down to temperature ~ 1 MeV, and was radiation-dominated. According to Friedmann equations,

$$H^2(t) = \frac{8\pi G}{3}\left[\rho(t) + \frac{\rho_{\rm cr} - \rho_0}{a^2(t)}\right], \tag{2.1}$$

which means that the energy density[1], ρ, drives the expansion rate of the Universe, $H = \dot{a}/a$, where a is the scale factor[2]. In radiation dominated era the contribution of relativistic particles dominates the total energy density, which is then expressed by $\rho = g_\star \frac{\pi^2}{30} T^4$, where T is the temperature of the plasma and

$$g_\star = \sum_{i=\text{bosons}} g_i \left(\frac{T_i}{T}\right)^4 + \frac{7}{8} \sum_{i=\text{fermions}} g_i \left(\frac{T_i}{T}\right)^4 \tag{2.2}$$

is the effective number of relativistic degrees of freedom (d.o.f.) [3, p 64]. Relativistic particles at the time were photons, electrons and positrons, constituting a thermal bath, and recently (although not yet completely) decoupled neutrinos (at a different temperature). Since $H \propto \sqrt{g_\star} T^2$, increases in $g_\star$ lead to a faster expansion rate and therefore to an earlier freeze out of the neutron-to-proton ratio, and eventually a higher primordial abundance of ^{4}He [3, p. 98]. The measurements and analysis of primordial ^{4}He mass fraction, Y_p, suggest that there may be a leftover d.o.f. of unknown origin, with the upper bound

$$\Delta g_\star = \sum_{i=\text{bosons}} g_i \left(\frac{T_i}{T}\right)^4 + \frac{7}{8} \sum_{i=\text{fermions}} g_i \left(\frac{T_i}{T}\right)^4 < 2.8\,, \tag{2.3}$$

where the sum runs over new bosons and fermions [4, p 45]. The above requirement opens up three possible scenarios: a) MCPs are either scalars or Majorana fermions; b) MCPs can be of any spin, if they froze out (just) before BBN, so that their temperature can be lower than that of the thermal bath; c) the production of MCPs must be suppressed up to BBN. In order to obtain the bounds, one assumes the latter statement. The general

[1] Present and critical values of energy density are denoted by ρ_0 and $\rho_{\rm cr}$, respectively.

[2] Scale factor shows how much the proper distance between two objects on fixed comoving coordinates grows over time. It is set to unity in current cosmological epoch.

idea is to write down rough estimates for production rate Γ, and then impose $\Gamma/H \lesssim 1$ at the relevant temperature. The result for millicharged fermions is $\epsilon < 2.1 \times 10^{-9}$ in the regime $m \lesssim m_e$ (m_e being the mass of electron) [5][6, p 6]. It is possible to avoid the BBN bounds on their charge altogether by assuming a non-zero lepton asymmetry [7].

Cosmic Microwave Background

As the temperature of the Universe dropped to ∼1 eV, Coulomb scattering ($e^- + p \leftrightarrow H + \gamma$) and Compton scattering ($e^-\gamma \rightarrow e^-\gamma$) were keeping the photons, electrons and protons tightly coupled [8, p 70]. Soon the former reaction was not efficient enough to maintain the equilibrium and thus neutral hydrogen formed leaving a progressively reduced free electron fraction. During this process, known as recombination, Thomson scattering ceased eventually due to lack of free electrons, and the photons decoupled altogether. The leftover radiation released around $T \sim 0.25$ eV is seen as Cosmic Microwave Background (CMB) today. The CMB energy spectrum corresponds to that of a nearly perfect black-body, the mean temperature of which is measured to a great accuracy by FIRAS and WMAP [9]. Recent Planck observations improved previously collected data of the small temperature anisotropies imprinted on CMB.

Any new particle with the mass $m \lesssim$ eV interacting with photons through a process $\gamma + \text{anything} \rightarrow X + \text{anything}$ would deplete the CMB energy spectrum in a frequency-dependent way [10]. This argument was used to rule out light MCPs with mass $\lesssim$ eV and charge $\epsilon \gtrsim 10^{-7}$. However, it is valid for only the post-decoupling epoch. Late time anisotropy effects have also been used to constrain MCP properties [11]. The idea is the following: CMB photons pass through a transverse magnetic field of galaxy clusters and get scattered by high energy electrons. This process, named Sunyaev-Zel'dovich effect, distorts the CMB spectrum as a function of frequency, reducing the number of low energy photons and increase the high energy photon one. Requiring that the extra flux reduction due to MCPs is not larger than that of the observed Sunyaev-Zel'dovich effect strongly constrains again a region of MCP parameter space, (m, q). CMB primary anisotropies also provide a bound on the cosmological abundance of MCPs, $\Omega_{\rm MCP}h^2$ [12]. If MCPs are sufficiently strongly coupled to baryons they participate in the acoustic oscillations of baryon-photon plasma during the recombination era. It is well known that any variation

in baryon abundance, $\Omega_b h^2$, changes the anisotropy spectrum [8, p 254]. The same applies to MCPs – at smaller angular scales the anisotropy spectrum would be suppressed if some fraction of baryons is replaced by MCPs. Because this is not observed, the abundance of tightly coupled MCPs must then be limited. Relevant simulations yield $\Omega_{\mathrm{MCP}} h^2 < 10^{-3}$.

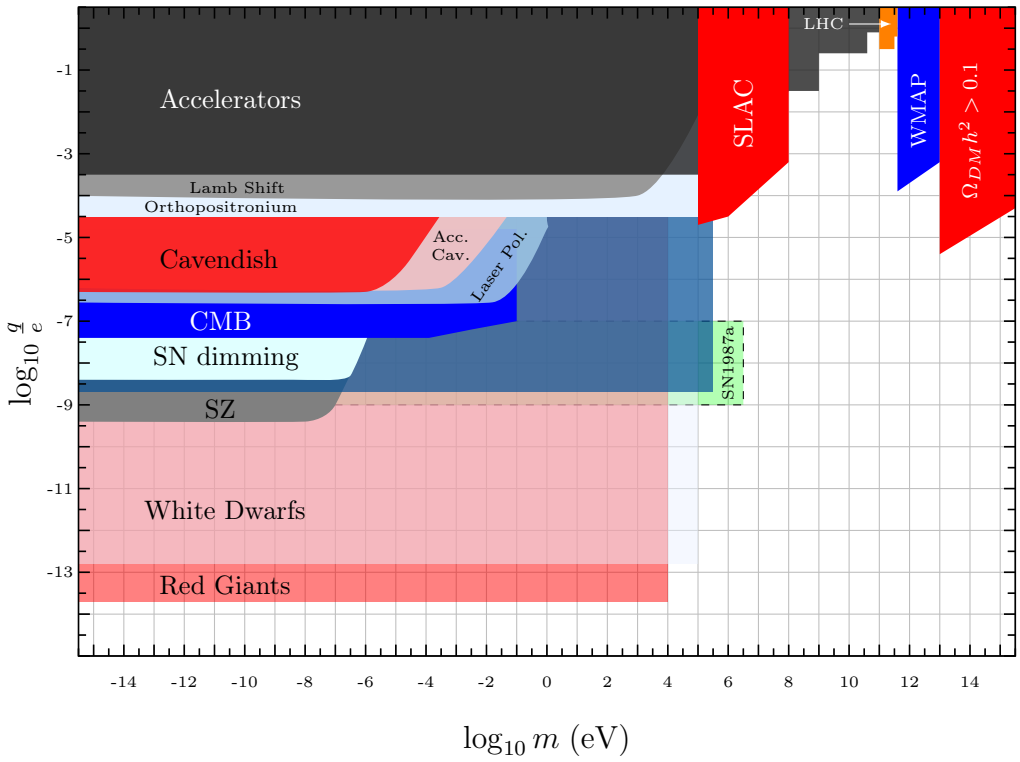

Figure 1: The constraints on MCPs with charge q and mass m. The compilation includes mostly millicharged fermion models without a paraphoton. One has to keep in mind that all the upper bounds are not derived under equal assumptions. Plot recreated from [13, p 116].

Miscellanea

A thorough review of astrophysical bounds are not subject to this thesis because it needs a lot of background information, but it is still reasonable to mention them, since the constraints arising from astrophysics cover a large region of the MCP parameter space (see fig. 1). The key common idea, though, is to include MCPs to the stellar evolution models and study their impact on various observables and parameters like total stellar luminosity, speed of the energy transfer from the core to surface, energy loss of the stars

etc [5, p 11][4, p 33]. Limits have been set from red giants, white dwarfs, supernova SN 1987A and horizontal branch (HB) stars (see [6, p 8] and references therein).

No study has been carried out yet to assess the effects of MCPs on opacity of the Universe and the CMB polarization. The Universe appears to be more transparent to very-high-energy photons than previously thought [14]. Investigating MCPs in this context might cast some bounds on MCPs.

2.2. Laboratory bounds

Accelerator cavities

Physicists in the first part of 20th century predicted that strong enough electromagnetic fields could lead to a spontaneous e^-e^+ pair production, also known as Schwinger pair production. The critical electric field strength above which the phenomenon could occur is reported to be $\mathcal{E}_c^e = \frac{m_e^2}{e} \simeq 1.3 \cdot 10^{18} \frac{\mathrm{V}}{\mathrm{m}}$, where m_e is electron's rest mass and e its charge. Electric field strengths that large are currently unreachable. However, if MCPs exist their corresponding critical electric field, $\mathcal{E}_c^{\mathrm{MCP}} = \frac{m^2}{q}$, may be attainable with today's technology. Since accelerator cavities employ electric fields $\mathcal{E}_0 \approx 100 \frac{\mathrm{MV}}{\mathrm{m}}$, the authors of [15] contemplated that MCPs may be produced there. If a large number of MCPs is produced (described by Schwinger formula), they would lead to a decrease in the cavity's quality factor (the energy stored in the cavity per energy loss due to dissipation and MCPs). Together with the orders-of-magnitude estimations this experiment leads to the bounds depicted in fig. 1.

Collider experiments

The only dedicated experiment in search for MCPs has been conducted at SLAC [16]. The so-called beam dump experiment was sensitive to MCPs with charge $\epsilon = 10^{-5} \ldots 0.1$ and mass $m = 0.1 \ldots 10^3\,\mathrm{MeV}$. A beam of electrons was shone at e^+-production target and the resulting products passed through $\sim$ 100m of sandstone. Muon chambers were placed between the target and the scintillation counter, the purpose of which was to detect MCPs. In principle, only MCPs should have been arrived to the detector. Cross-checking the measurements against expected number of MCPs led to a conclusion that such particles

with mass and charge relevant to the experiment do not exist.

Optical experiments

If any novel particles are coupled to photons, optical experiments, such as PVLAS, BFRT and Q&A, could provide evidence for physics beyond SM. The setup of PVLAS is simple: a linearly polarized laser beam passes through vacuum where a strong transverse magnetic field is applied and the changes in polarization is then analyzed [17]. Rotation of the polarization plane and phase difference translates into dichroism and birefrigence of the vacuum, respectively, which means that that vacuum develops a complex refractive index. It is theorized that the interaction between the external magnetic field and a photon from the laser beam leads to the so-called photon splitting $\gamma \to e^+e^-$ and modify refractive index of the vacuum [4, p 17]. The threshold energy for the laser beam must exceed $2m_e$ for this particular process [18]. However, the birefrigence, Δn, could be detected without meeting this requirement if the external magnetic field is comparable to its critical value $B_c = \frac{m_e^2}{e}$.

With these considerations in mind, it is natural to assume that any new light particle coupled to the photons could modify vacuum refractive index below the limits set by QED. Since $\Delta n = \Delta n(m, q) < 10^{-19}$, it follows that optical experiments strongly constrain the existence of light MCPs with mass $m \gtrsim 0.1\,\mathrm{eV}$ and charge $\epsilon \gtrsim 10^{-6}$ [18]. It should be noted that in 2006, the PVLAS collaboration erroneously claimed on observed polarization change orders of magnitude larger than expected [19]. This was followed by a series of articles trying to explain the phenomena, possibly underestimating the bounds on MCPs.

Radiative corrections and orthopositronium decay

Dirac's theory predicts a magnetic moment of an electron to be $g_e = 2$, but its radiative corrections induce a slight deviation from this value (see fig. 2). The QED calculations of the small shift, called anomalous magnetic moment, are well in accordance with the measurements up to 10 significant figures. Any new particle coupled to the photon should contribute to electron-photon vertex function. This in turn allows to set constraints on its charge (because photons couple to only charged particles) and mass, as it is done in [4, p 52]. The expression used to estimate the bounds was derived in [20], the leading

contribution of which is

$$a_e = \delta\left(\frac{g_e - 2}{2}\right) = \frac{\epsilon^2}{3}\left(\frac{\alpha}{\pi}\right)^2 \log\frac{m_e}{m}\,,$$

where $\alpha = \frac{e^2}{4\pi}$ stands for the fine structure constant.

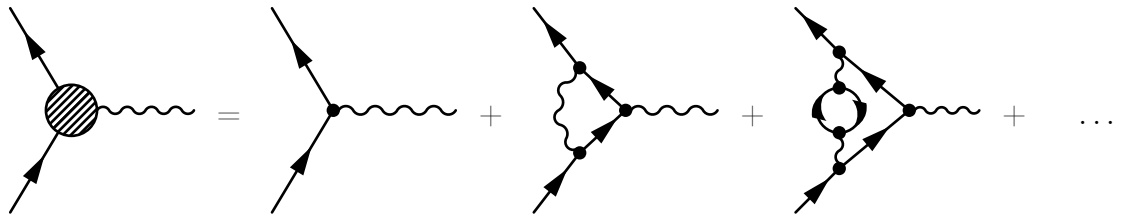

Figure 2: Electron-photon coupling beyond leading-order of perturbation theory (first summand). The vertex function also includes vacuum polarization created by an MCP pair (third summand).

Lamb shift is a small energy difference between two hydrogen energy levels $^2S_{1/2}$ and $^2P_{1/2}$. According to Dirac's theory the energy levels should be degenerate, however, vacuum fluctuations again modify the classical behavior (Coulomb potential). The expected energy difference due to MCPs,

$$\Delta E_{\text{Lamb}} = E(^2S_{1/2}) - E(^2P_{1/2}) \overset{m\lesssim 1\,\text{keV}}{\approx} -\frac{\alpha^3 m_e}{18\pi}\epsilon^2\,,$$

must be less than the discrepancy between QED predictions and measurements, which yields $\epsilon \leq 1.085 \times 10^{-4}$ for $m \lesssim 1\,\text{keV}$ [21]. Despite the the fact that the anomalous magnetic moment has been measured more precisely than the Lamb shift, the bounds are weaker because MCPs contribute to the Lamb shift at one loop but to a_e at two loops.

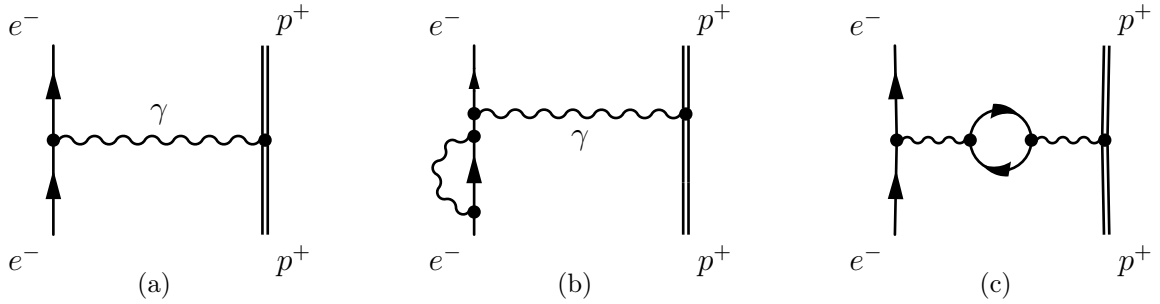

Figure 3: (a) Classical electron-proton interaction. (b) Lamb shift due to electron mass renomralization. (c) Energy shift caused by virtual MCP pairs.

Finally, limits have also been set from orthopositronium (o-Ps) decay, which is a spin-1 bound state of an electron and a positron. Since spin-1 particles cannot decay into even number pair of photons due to Landau-Yang theorem [22], the only possibilities are o-Ps $\to$ odd γ, with o-Ps $\to 3\gamma$ being the dominant one. The author of [23] found that the decay rate for o-Ps $\to$ MCPs is

$$\Gamma(\text{o-Ps} \to \text{MCPs}) = \epsilon^2 \frac{m_e \alpha^6}{6} \sqrt{1 - \frac{m^2}{m_e^2}} \left(1 + \frac{m^2}{m_e^2}\right) \overset{m<m_e}{\approx} \epsilon^2 \frac{m_e \alpha^6}{6} \,.$$

The branching ratio of o-Ps into invisible particles has been measured to be

$$\text{BR}(\text{o-Ps} \to \text{invisible}) = \frac{\Gamma(\text{o-Ps} \to \text{invisible})}{\Gamma(\text{o-Ps} \to 3\gamma)} < 4.2 \cdot 10^{-7} \,,$$

thus giving the bounds $\epsilon < 3.4 \cdot 10^{-5}$ for $m < m_e$ [24].

3. Process $\gamma\gamma \to$ MCPs

The premise of this section is that MCPs are additional particles interacting only with the photons. MCPs annihilate and are produced through the process $\gamma\gamma \leftrightarrow$ MCPs which is the basis for casting the bounds on MCPs presented in the next chapter. A more general (unified) theory would allow additional interactions like $e^+e^- \to$ MCPs that would help to place stricter bounds on MCPs. For instance, the cross-section of photon annihilation would be proportional to q^4/m^2 whereas for electron-positron annihilation it would be q^2e^2/m^2. As we will show, a larger cross-section leads to a smaller relic abundance of MCPs which must not be larger than that of dark matter. For the sake of simplicity, any other process than $\gamma\gamma \leftrightarrow$ MCPs is neglected here. The assumption is valid in certain mass and charge region of MCPs where the considered process is dominant.

The emphasis here lies on vector boson MCPs since scalar and fermion cases reduce to the special cases of scalar and fermion QED which have been thoroughly investigated in the past (the summary is given in the appendix A.2).

3.1. Lagrangian

A millicharged vector boson is a spin-1 particle with a small electric charge $q \equiv \epsilon e$ and is, thus, coupled to the photon. Due to the conservation of electric charge there also must be an antiparticle with the charge of opposite sign. The Lagrangian describing MCPs and their interactions with photons is assumed to be symmetric under $U(1)$ gauge transformations (just like electromagnetism). Specifically, the transformation laws are

$$\begin{aligned} W_\mu^+ \equiv \;& W_\mu \to e^{iq\alpha} W_\mu && \text{for the particle}\,, \\ W_\mu^- \equiv \;& W_\mu^\dagger \to e^{-iq\alpha} W_\mu^\dagger && \text{for its antiparticle}\,, \\ & A_\mu \to A_\mu - \partial_\mu \alpha && \text{for the photon}\,. \end{aligned} \tag{3.1}$$

The Lagrangian of free charged massive vector field (also known as Proca field) can be written as

$$\mathcal{L}_{\text{free}} = -\frac{1}{2} V_{\mu\nu}^\dagger V^{\mu\nu} + m^2 W_\mu^\dagger W^\mu\,,$$

where m is mass of the particle and $V_{\mu\nu} = \partial_\mu W_\nu - \partial_\nu W_\mu$ its field strength tensor. Minimal substitution, in which the partial derivative is replaced by covariant one,

$$V_{\mu\nu} \to W_{\mu\nu} = D_\mu W_\nu - D_\nu W_\mu \,,$$

with $D_\mu = \partial_\mu + iqA_\mu$, introduces electromagnetic interaction to the theory and ensures its invariance under (3.1). After applying the substitution, the Lagrangian has now two additional interaction terms (plus the kinetic term for the photon field):

$$\begin{aligned} \mathcal{L}_{\text{mc}} = \mathcal{L}_{\text{free}} - \frac{1}{4} F_{\mu\nu} F^{\mu\nu} + \\ + iq(V^{\mu\nu} A_\mu W_\nu^\dagger - V_{\mu\nu}^\dagger A^\mu W^\nu) + q^2 (A^\mu W_\mu^\dagger A^\nu W_\nu - A^\mu A_\mu W^\nu W_\nu^\dagger) \,. \end{aligned} \tag{3.2}$$

Any theory of massive particles minimally interacting with photons would lead to unitarity violation of the S-matrix at high energies [25] [1]. The problem is solved by adding other (non-minimal) interaction terms to the Lagrangian so that it still retains the local $U(1)$ symmetry (and meets the basic requirements of a Lagrangian [26, pp. 77-82]). Noticing that D_μ and hence $W_{\mu\nu}$ obtain a phase under the $U(1)$ transformation just as the basic fields in (3.1), the final Lagrangian with all such possible interaction terms reads[2]

$$\begin{aligned} \mathcal{L} = &- \frac{1}{4} F^{\mu\nu} F_{\mu\nu} - \frac{1}{2} W_{\mu\nu}^\dagger W^{\mu\nu} + m^2 W_\mu^\dagger W^\mu + && \text{(minimal coupling)} \\ &+ iq W_\mu^\dagger W_\nu (g_1 F^{\mu\nu} + g_2 \widetilde{F}^{\mu\nu}) + \xi D_\mu W^\mu (D_\nu W^\nu)^\dagger + && \text{(non-minimal terms)} \\ &+ \chi_1 W^\mu W_\mu^\dagger W^\nu W_\nu^\dagger + \chi_2 W_\mu W^\mu W_\nu^\dagger W^{\nu\dagger} && \text{(self-scattering)} \,. \end{aligned} \tag{3.3}$$

Any pseudoscalars (terms involving pseudo-quantities like dual tensors) in Lagrangian introduces parity violation to the theory. A term like $D^\mu W^\nu (D_\mu W_\nu)^\dagger$ is proportional to $W^{\mu\nu} W_{\mu\nu}^\dagger$ and hence neglected. It turns out that $W^{\mu\nu} \widetilde{W}_{\mu\nu}^\dagger \propto \widetilde{F}^{\mu\nu} W_\mu^\dagger W_\nu$ and can be excluded as well since it doesn't describe any new dynamics (see appendix A.1.1). It is not possible to add more terms involving MCPs without spoiling the gauge invariance, because terms like $W^{\mu\nu} W_{\mu\nu}$, $F^{\mu\nu} W_\mu W_\nu$ and their complex conjugates obtain a phase under $U(1)$ transformations.

[1] This basically means that the sum of all probabilities for the process $|i\rangle \to |f\rangle$ exceeds 1, which then leads to unbounded cross-section.

[2] $\widetilde{F}^{\mu\nu}$ is the dual tensor of $F^{\mu\nu}$ with the definition $\widetilde{F}_{\mu\nu} \equiv \frac{1}{2} \epsilon_{\mu\nu\rho\sigma} F^{\rho\sigma}$, where $\epsilon^{\mu\nu\rho\sigma}$ is the Levi-Civita symbol.

The relevant Feynman diagrams are given in fig. 4. Terms proportional to q contribute to 3.4(a), $\propto q^2$ generates the diagram 3.4(b), and 3.4(c) stands for the self-scattering terms. It will be ignored in the following calculations because only photon-MCP interactions are of interest here (meaning that $\chi_1 = \chi_2 = 0$).

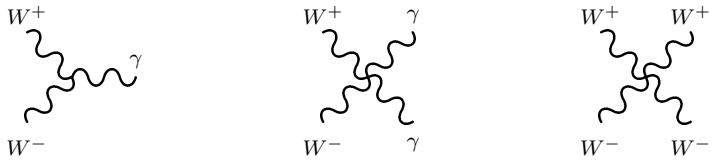

Figure 4: Feynman diagrams for millicharged vector bosons.

In order to arrive at a quantitatively meaningful result, the parameters ξ, g_1 and g_2 needs to be fixed. It turns out that the Lagrangian resulting from the minimal substitution, $\mathcal{L}_{\text{mc}}$ (3.2), already contains the term $W_\mu^\dagger W_\nu F^{\mu\nu}$ (see A.1.1 for proof). In the non-relativistic approximation it reduces to $\boldsymbol{\mu} \cdot \mathbf{B}$, where $\mathbf{B}$ is magnetic field, $\boldsymbol{\mu} = g_m \frac{q}{2m} \mathbf{S}$ magnetic moment of MCPs and $\mathbf{S}$ their spin operator. There exist arguments from the realm of low- and high-energy Compton scattering, which suggest that the „natural" Lande g-factor, g_m, for an electromagnetically charged particle of any spin must be two [25][27, p. 322], but $\mathcal{L}_{\text{mc}}$ leads to $g_m = 1$ [28]. Therefore the g_1-term in the full Lagrangian (3.3) is required in order to increase the g-factor to its natural value. In general the g-factor and the coupling constant g_1 are related by $g_1 = g_m - 1$. Hence, a proper choice of parameters is $g_1 = 1$, $g_2 = 0$ and $\xi = -1$, ensuring no explicit parity violation.

The explicit calculations of the equations of motion (A.4) and the Noether current (A.5) resulting from the theory are given in A.1.1.

3.2. Invariant matrix element

The S-matrix is an operator that relates asymptotic initial and final states of a scattering process in such a way that its elements represent the probability amplitude of the process. By subtracting the non-interacting part (particles passing through each other) from it and factoring out the conservation of momentum, one is left with invariant matrix element $\mathcal{M}$ (also known as the scattering amplitude) which contains all dynamics of the transition between the initial and final states. This element is used in the calculations of cross-section

and decay rates.

Apart from the fact that Feynman diagrams are helpful in visualizing certain processes, they are also used as a tool to write down the correct $\mathcal{M}$ of the process without much effort. To do so, all possible transitions the Lagrangian permits must be considered.

The tree-level (i.e. leading order) matrix element for the process $\gamma\gamma \to W^+W^-$ is depicted in fig. 5. In order to write down a proper expression for $\mathcal{M}$, a set of Feynman rules are needed. The key points of deriving these rules, outlined in [29, pp. 428-431], are:

a) select all relevant interaction parts of the Lagrangian that describe a particular vertex;
b) draw the diagram and set a direction of the momentum on each line;
c) write down the interaction Lagrangian in terms of polarization vectors (while ignoring polarization state for the moment);
d) collect the indices and momenta, obtain the vertex factor.

The prescription is applied to the diagrams 3.4(a) and 3.4(b), which produces the rules $\mathcal{M}^{\alpha\beta\gamma}(j,\, k,\, l)$ (A.6) and $\mathcal{M}^{\alpha\beta\mu\nu}$ (A.7).

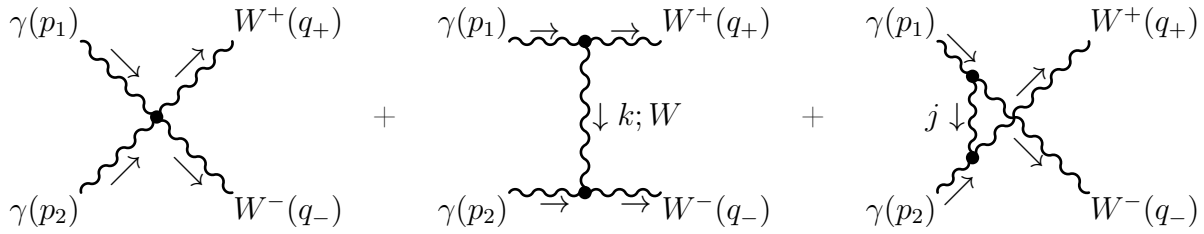

Figure 5: Leading order contributions of the process $\gamma\gamma \to W^+W^-$. The arrows represent the direction of four-momentum.

As it can be seen from the last two diagrams in fig. 5, the amplitude contains a virtual (i.e. off-shell) MCP state called propagator. Its expression (derived in A.1.1) reads

$$D^F_{\alpha\beta}(p) = \ ^{\alpha}\!\sim\!\!\!^{p}\!\!\sim\!^{\beta} \ = \frac{P_{\alpha\beta}(p)}{p^2 - m^2} - \frac{\xi}{\xi p^2 + m^2} \cdot \frac{p_\alpha p_\beta}{m^2}\,,$$

$$\text{where} \quad P_{\alpha\beta}(p) = \sum_{p^\mu \epsilon_\mu = 0} \epsilon_\alpha(p)\epsilon^*_\beta(p) = \frac{p_\alpha p_\beta}{m^2} - g_{\alpha\beta} \tag{3.4}$$

is the polarization projection operator. This operator projects out the subspace spanned by MCP polarization vectors $\epsilon^r_\mu(p)$ $(r = 1, 2, 3)$ which are orthogonal to the momentum

p_μ if the massive vector boson is on-shell. Since the amplitude for a particle to be created with momentum p and polarization r is proportional to $\epsilon^r_\alpha(p)$, and the amplitude for it to be annihilated is proportional to $\epsilon^{*r}_\beta(p)$, the projection operator represents the spin correlation between the initial and final state. Constant ξ could be considered as a „gauge fixing" parameter.

The invariant matrix element can be now written as

$$\mathcal{M} = \varepsilon_\alpha(p_1)\varepsilon_\beta(p_2)\epsilon_\mu(q_+)\epsilon^*_\nu(q_-)\mathcal{M}^{\alpha\beta\mu\nu}(p_1,\, p_2,\, q_+,\, q_-)\,, \tag{3.5}$$

where

$$\begin{aligned}\mathcal{M}^{\alpha\beta\mu\nu}(p_1,\, p_2,\, q_+,\, q_-) = \mathcal{M}^{\alpha\beta\mu\nu} + \mathcal{M}^{\mu\lambda\alpha}(-q_+, -k, p_1)iD^F_{\lambda\sigma}(k)\mathcal{M}^{\sigma\nu\beta}(k, -q_-, p_2) + \\ + \mathcal{M}^{\lambda\nu\alpha}(-j, -q_-, p_1)iD^F_{\lambda\sigma}(j)\mathcal{M}^{\mu\sigma\beta}(-q_+, j, p_2)\,.\end{aligned} \tag{3.6}$$

Since the momentum must be conserved in every vertex, it must be the case that

$$p_1 + p_2 - q_+ - q_- = 0\,, \quad k = p_1 - q_+ = q_- - p_2\,, \quad j = p_1 - q_- = q_+ - p_2\,. \tag{3.7}$$

3.3. Cross-section

The likelihood of some particular interaction can be measured by counting the number of produced particles f_ψ per unit time normalized to the flux of incoming particles i_ψ. The result gives the cross-section σ of all possible interactions for the process $i_\psi \to f_\psi$.

The differential cross-section of a two-particle process, $a + b \to 1 + 2$, can be written as

$$\frac{\mathrm{d}\sigma}{\mathrm{d}t} = \frac{|\mathcal{M}_{fi}|^2\,\Theta(s - s_{\min})}{16\pi\lambda(s, m_a^2, m_b^2)}\,, \tag{3.8}$$

where $\lambda(x, y, z)$ is Källen function (A.1) and s, t Mandelstam variables (A.2) [30, p. 26]. Since the initial and final particles must be on-shell, the minimum center of momentum (c.m.) energy for the interaction to take place is determined by the masses of the latter. In other words, if initial energy is not high enough, the final states would not be created (and vice versa). That's why there is a Heaviside function, $\Theta(s - s_{\min})$, in (3.8) with $s_{\min} = (m_1 + m_2)^2$.

The information about polarization is encoded in the scattering amplitude, $\mathcal{M}_{fi}$. If we are not interested in the polarized cross-section, then we average $|\mathcal{M}_{fi}|^2$ over the initial and sum over the final polarization states in order to get the unpolarized cross-section.

Unpolarized cross-section

Since the photon is a massless boson and has only two degrees of freedom due to gauge fixing, the sum over its polarization states isn't given by (3.4). Instead Ward identity applies here [29, p. 135], yielding

$$\sum_{r=1,2} \varepsilon_\mu^r \varepsilon_\nu^r \to -g_{\mu\nu}\,.$$

The unpolarized cross-section for $\gamma\gamma \to$ MCPs now reads[3]

$$\frac{\mathrm{d}\overline{\sigma}}{\mathrm{d}t} = \frac{\overline{|\mathcal{M}_{fi}|^2}\Theta(s-4m^2)}{16\pi\lambda(s,0,0)} = \frac{\Theta(s-4m^2)}{64\pi s^2} g_{\alpha\alpha'} g_{\beta\beta'} \mathcal{A}^{\alpha\beta\alpha'\beta'}(p_1^*,\, p_2^*,\, q_+^*,\, q_-^*)\,, \tag{3.9}$$

where

$$\mathcal{A}^{\alpha\beta\alpha'\beta'}(p_1^*,\, p_2^*,\, q_+^*,\, q_-^*) = P_{\mu\mu'}(q_+^*) P_{\nu\nu'}(q_-^*) \mathcal{M}^{\alpha\beta\mu\nu}(p_1^*,\, p_2^*,\, q_+^*,\, q_-^*) \mathcal{M}^{*\,\alpha'\beta'\mu'\nu'}(p_1^*,\, p_2^*,\, q_+^*,\, q_-^*)\,.$$

The total cross-section is just a matter of integration using the limits (A.3). Explicit calculations performed with the FeynCalc package[4] give

$$\overline{\sigma}(\beta) = \frac{\overline{\sigma}_\infty}{16}\left[\beta\left(22 - 9\beta^2 + 3\beta^4\right) - 3\left(1-\beta^2\right)\left(1-\beta^4\right)\operatorname{atanh}\beta\right]\,, \tag{3.10}$$

where $\beta = \sqrt{1-\frac{4m^2}{s}}$ is the velocity of MCPs in c.m. frame and $\overline{\sigma}_\infty$ its asymptotic high energy limit:

$$\overline{\sigma}_\infty \equiv \lim_{\beta\to 1} \overline{\sigma}(\beta) = \frac{q^4}{2\pi m^2}\,. \tag{3.11}$$

The behavior of (3.10) is depicted in fig. 6.

[3] The asterisks denote that the momenta is chosen in a particular frame of reference.

[4] A Mathematica package for symbolic HEP calculations – http://www.feyncalc.org/.

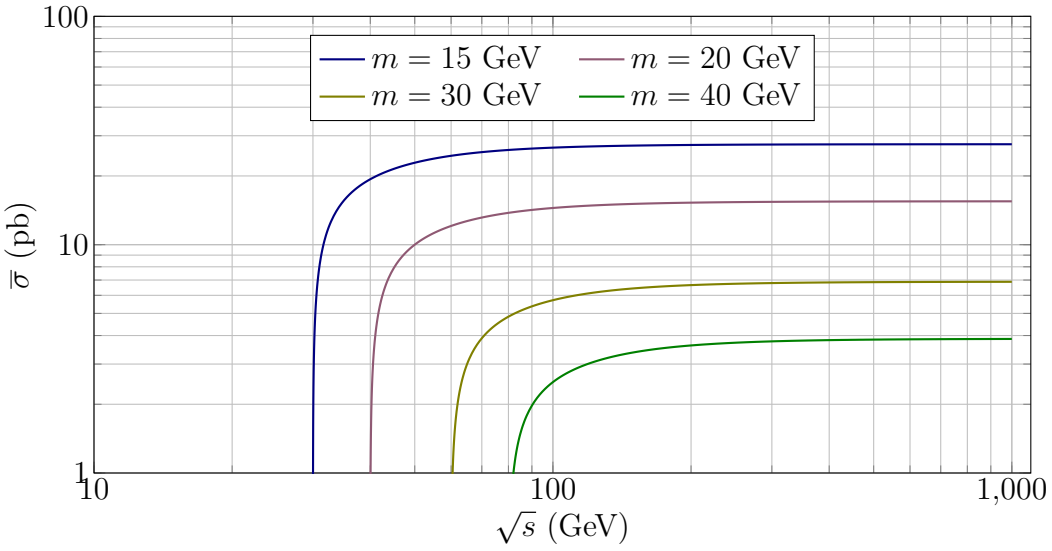

Figure 6: Total cross-section of the process $\gamma\gamma \to W^+W^-$. The millicharge is set to one-tenth of the elementary charge.

Polarized cross-section

The polarized cross-section takes the polarization states of initial photons into account. The corresponding amplitude can be written as

$$\mathcal{M}_{r_1 r_2}(p_1^*,\, p_2^*,\, q_+^*,\, q_-^*) = \varepsilon_\alpha^{r_1}(p_1^*)\varepsilon_\beta^{r_2}(p_2^*)\mathcal{M}^{\alpha\beta}(p_1^*,\, p_2^*,\, q_+^*,\, q_-^*)\,,$$

where $r_{1,2} \in \{-,\, +\}$ denote left- and/or right-handed polarization states of the initial photons. By using the polarization projection tensors, $P^r_{\mu\nu}(p,\, q) = \varepsilon^r_\mu(q)\varepsilon^{*r}_\nu(q)$, to project out relevant helicity states, and summing over final spin states, the differential cross-section for the process takes the form

$$\begin{aligned}
\mathrm{d}\sigma_{r_1 r_2} &= \frac{\mathrm{d}t\;\Theta(s-4m^2)}{16\pi s^2}\;\left|\mathcal{M}_{r_1 r_2}(p_1^*,\, p_2^*,\, q_+^*,\, q_-^*)\right|^2 = \\
&= \frac{\mathrm{d}t\;\Theta(s-4m^2)}{16\pi s^2}\;P^{r_1}_{\alpha\alpha'}(p_1^*+p_2^*,\, p_1^*)P^{r_2}_{\beta\beta'}(p_1^*+p_2^*,\, p_2^*)\;\mathcal{A}^{\alpha\beta\alpha'\beta'}(p_1^*,\, p_2^*,\, q_+^*,\, q_-^*)\,.
\end{aligned}$$

As shown in appendix A.1.2, the photon projector operator can be written as

$$P^r_{\mu\nu}(p,\, q) = \frac{1}{2}\left[P_{\mu\nu}(p,\, q) + rF_{\mu\nu}(p,\, q)\right]\,, \tag{3.12}$$

where

$$P_{\mu\nu}(p,\, q) = \frac{p_\mu q_\nu + p_\nu q_\mu}{p\cdot q} - g_{\mu\nu} \quad \text{and} \quad F_{\mu\nu}(p,\, q) = \frac{i\epsilon_{\mu\nu\rho\sigma}p^\rho q^\sigma}{p\cdot q}\,. \tag{3.13}$$

Due to Ward identity again, $P_{\mu\nu}(p,\, q)$ reduces to $-g_{\mu\nu}$ once contracted with the scattering amplitude. This leads to a polarized differential cross-section of the form

$$\begin{aligned}
\mathrm{d}\sigma_{r_1 r_2} &= \tfrac{1}{4}\tfrac{\mathrm{d}t\;\Theta(s-4m^2)}{16\pi s^2}\,\mathcal{A}^{\alpha\beta\alpha'\beta'}\left[g_{\alpha\alpha'} + r_1 F_{\alpha\alpha'}(p_1^*+p_2^*,\, p_1^*)\right]\cdot\left[g_{\beta\beta'} + r_2 F_{\beta\beta'}(p_1^*+p_2^*,\, p_2^*)\right] = \\
&= \tfrac{1}{4}\tfrac{\mathrm{d}t\;\Theta(s-4m^2)}{16\pi s^2}\mathcal{A}^{\alpha\beta\alpha'\beta'}\;\left[g_{\alpha\alpha'}g_{\beta\beta'} + r_1 g_{\beta\beta'}F_{\alpha\alpha'}(p_1^*,\, p_2^*) - r_2 g_{\alpha\alpha'}F_{\beta\beta'}(p_1^*,\, p_2^*) - \right. \\
&\qquad\qquad \left. - r_1 r_2 F_{\alpha\alpha'}(p_1^*,\, p_2^*)F_{\beta\beta'}(p_1^*,\, p_2^*)\right] = \\
&\equiv \mathrm{d}\left(\overline{\sigma} + r_1\sigma_1 + r_2\sigma_2 + r_1 r_2\sigma_{12}\right)\,.
\end{aligned}$$

So, instead of finding the same projections and contractions all over again for each helicity configuration, it is computationally more effective to reuse temporary results, $\overline{\sigma}$, σ_1, σ_2 and σ_{12}, and find the polarized cross-sections with these (see appendix A.1.3).

Since the momenta of photons are back-to-back in the c.m. frame, their spins are (anti)aligned if the sign of their helicities have (not) different signs. In other words, configurations like $++$ and $--$ have antiparallel spins whereas for $+-$ and $-+$ the spins are parallel. It follows that for a P-symmetric Lagrangian the measurements of observables do not change if all momenta is mirrored or, equivalently, if the signs of helicities are flipped. Thus, if $g_2 = 0$ then $\sigma_{++} = \sigma_{--}$ and $\sigma_{+-} = \sigma_{-+}$. Since this is the case the total polarized cross-section can be written as

$$\sigma_{r_1 r_2} = \overline{\sigma}\left(1 + A r_1 r_2\right)\,, \quad \text{where} \quad A = \frac{\sigma_{12}}{\overline{\sigma}} \tag{3.14}$$

stands for spin asymmetry. The integration of $\mathrm{d}\sigma_{12}$ yields

$$\sigma_{12} = \frac{\overline{\sigma}_\infty}{16}\left(1-\beta^2\right)\left[2\left(3+5\beta^2\right)\operatorname{atanh}\beta - 19\beta\right]\,. \tag{3.15}$$

Resulting polarized cross-sections are plotted in fig. 8.

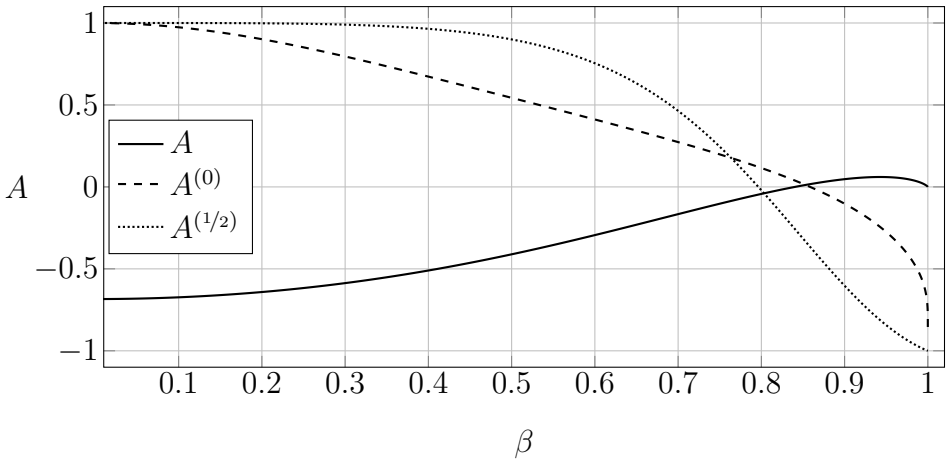

Figure 7: Asymmetry (3.14) as a function of velocity β of MCPs. At the threshold the asymmetry for vector MCPs is the largest whereas at higher energies it asymptotically goes to zero – the difference between polarized and unpolarized cross-sections becomes insignificant. For scalar (dashed) and fermion (dotted) MCPs the asymmetry flips the sign ($1 \to -1$).

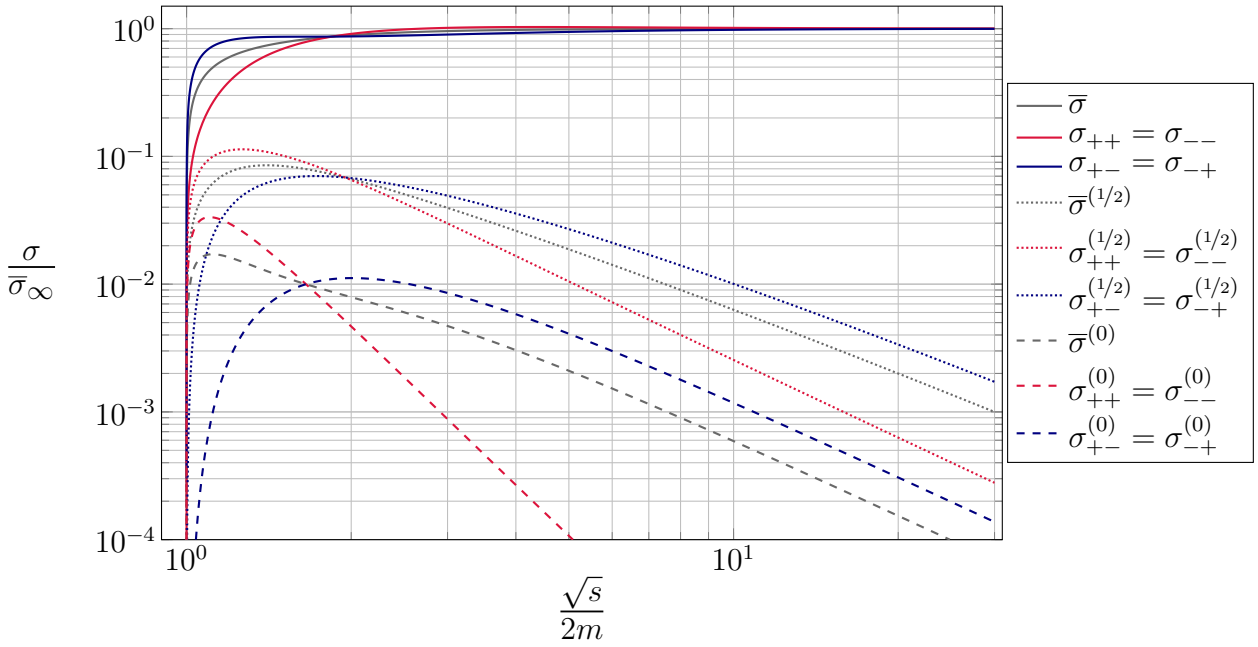

Figure 8: Normalized total unpolarized and polarized cross-sections. The cross-section for vector boson MCPs (solid line) approaches to a constant non-zero value unlike scalar boson (dashed) and fermion (dotted) MCPs which approach to zero. The Lagrangian, Feynman diagrams and cross-sections for scalar and fermion MCPs are given in A.2.

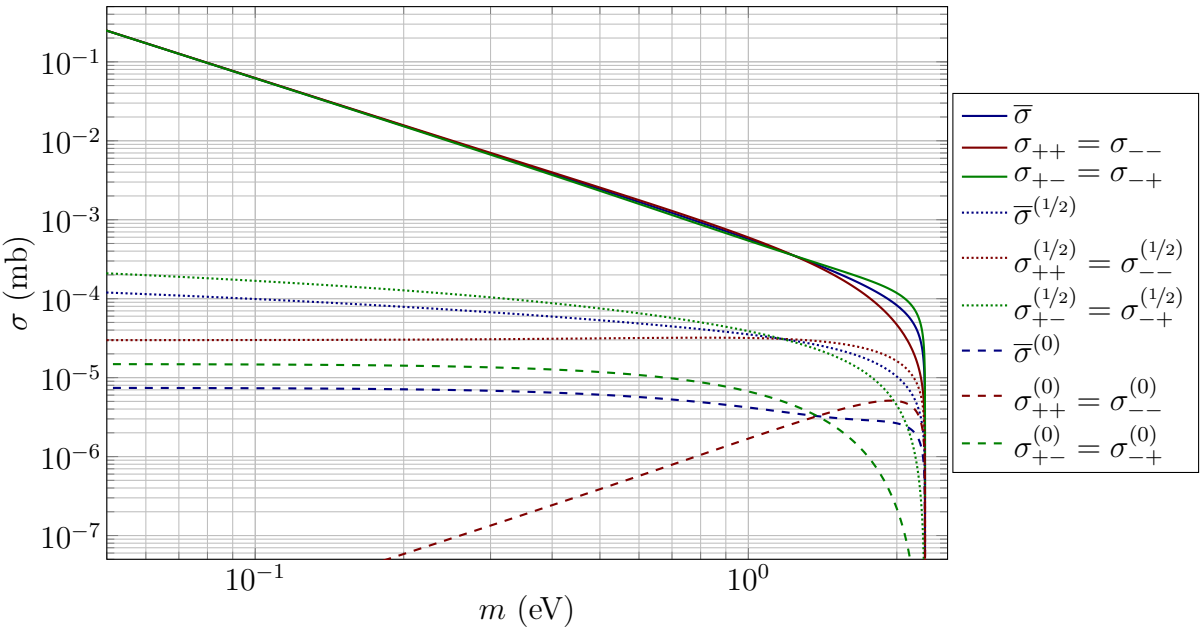

Figure 9: Mass dependence of cross-sections at $q = 10^{-5}e$. The initial photons have a wavelength of 543.5 nm (2.28 eV), the average wavelength of a He-Ne (green) laser.

4. Constraints on MCPs from Boltzmann equation

The Universe, in its earliest stages, was a hot and dense thermal bath comprised of bosons and relativistic fermions. The Universe started to cool down due to the expansion[1]. The primordial soup maintained local thermal equilibrium as long as the interactions, namely scatterings, between its constituents were rapid enough to overcome the expansion rate.

As the Universe expands, at some point the mean free path $\overline{\lambda}$ of a species initially coupled to the thermal bath drops below Hubble radius H^{-1}. Their interaction rate Γ is not high enough to maintain the equilibrium (because $\Gamma \sim \overline{\lambda}^{-1}$) and eventually they decouple from the plasma. Consequently, there will be a relic abundance of these particles. The important point is that the decoupling is inherently a non-equilibrium process, and must be treated with the Boltzmann equation,

$$\frac{\mathrm{d}n}{\mathrm{d}t} + 3Hn = -\frac{\langle\sigma v\rangle}{2}\left(n^2 - n_{EQ}^2\right) . \tag{4.1}$$

Here n and n_{EQ} are number density and equilibrium number density of MCPs, which encodes the effects of annihilation and production of these particles, respectively[2]. We assume that the abundances of MCPs and their antiparticles are equal ($n_+ = n_-$), and consider their sum in the Boltzmann equation ($n = n_+ = n_-$), hence the factor $\frac{1}{2}$ in (4.1).

The expansion of the Universe causes dilution of the number density, hence the $3Hn$ term in LHS of (4.1). The interaction rate is proportional to the cross-section of the process, which depends on the c.m. energy, the distribution of which in turn is governed by the temperature of the thermal bath. In other words, the cross-section needs to be thermally averaged, and that is what the $\langle\sigma v\rangle$ term stands for. The Boltzmann equation, (4.1), already includes implicit assumptions like local thermal equilibrium (i.e. kinetic and chemical equilibrium) which in a nutshell means that the annihilation products go quickly into equilibrium with the thermal bath, and the time reversal invariance of the interaction [3, pp. 117-120].

[1] The temperature of the plasma, T, is often identified with that of the photons. The change of temperature in time is governed by expansion of the Universe as $\dot{T} = -HT$.

[2] Ignoring the diluting term for a moment, we see that if $n < n_{EQ}$, then $\dot{n} > 0$ and production of the particles prevails. On the other hand, if $n > n_{EQ}$, then $\dot{n} < 0$ and their annihilation dominates.

The aim of this section is to find out how does the relic density of MCPs depend on their mass and charge. The relic density should be proportional to the physical abundance of the particles in today's Universe. Assuming that MCPs comprise all of dark matter, the physical abundance of which is known, it is possible to place some bound their mass and charge. The initial abundance of MCPs is assumed to be negligible.

4.1. Equilibrium density

The equation (4.1) can be expressed in (dimensionless) number density of particles per comoving volume[3], $Y = \frac{n}{n_\gamma}$, where $n_\gamma = \frac{2\zeta(3)}{\pi^2}T^3$ is the photon number density. It is customary to introduce another dimensionless quantity as the independent variable, $x = \frac{m}{T}$. If the freeze-out of MCPs occurs in the radiation dominated era, the Hubble rate takes the from $H(T) = \sqrt{\frac{4\pi^3}{45}g_*(T)}\frac{T^2}{m_{\mathrm{Pl}}}$, where $m_{\mathrm{Pl}} = \sqrt{\frac{\hbar c}{G}}$ is the Planck mass [3, p. 64]. It can be showed that

$$\langle\sigma v\rangle(x) = \frac{4x}{K_2^2(x)}\int_1^\infty \mathrm{d}y\, \overline{\sigma}(4m^2y)\sqrt{y}(y-1)K_1(2x\sqrt{y})\,, \tag{4.2}$$

where $y = \frac{s}{4m^2}$ and $K_n(x)$ is n-th modified Bessel function of the second kind (B.1) [31, p. 152].

Thus, the Boltzmann equation can be recast into a more concise form,

$$Y' = -\lambda\langle\sigma v\rangle_f(x)x^{-2}\left[Y^2 - \left(Y_{EQ}^{(\eta)}\right)^2\right], \tag{4.3}$$

where $\langle\sigma v\rangle_f$ is thermally averaged cross-section normalized to the asymptotic value of spin-1 MCP cross-section, $\overline{\sigma}_\infty$ (3.11), and

$$\lambda(q,\, m) = \frac{q^4}{m}\alpha\,, \quad \alpha = \frac{3\zeta(3)}{4\pi^4}\sqrt{\frac{5}{\pi}}g_*^{-\frac{1}{2}}m_{\mathrm{Pl}}\,. \tag{4.4}$$

The integration limits are $x_r \ldots x_0$ where

$$x_r = \frac{m}{T_{RH}} \quad \text{and} \quad x_0 = \frac{m}{T_0}\,. \tag{4.5}$$

We assume that all the SM particles are in equilibrium in the plasma at the reheating temperature, T_{RH}. The MCP production was then triggered by the process $\gamma\gamma \to$ MCPs.

[3]For the sake of simplicity, from now on „number density" is used instead of its verbose (but correct) name.

Although the MCPs departed from the thermal bath later, the Boltzmann equation describes their number density up until today. The temperature of the Universe today is $T_0 = 2.73\ \mathrm{K} = 2.35 \cdot 10^{-4}\ \mathrm{eV}$ – hence the integration limits.

The equilibrium number density depends on whether MCP is either a fermion ($\eta = 1$) or a boson ($\eta = -1$):

$$Y_{EQ}^{(\eta)}(x) = \frac{g}{4\zeta(3)} x^2 \sum_{n=1}^{\infty} \frac{K_2(nx)}{n} (-\eta)^{n-1}\,, \tag{4.6}$$

where g accounts for d.o.f. of the particle (for a derivation see B.2). As fig. 10 shows, the discrepancy between the distributions becomes remarkable at $x < 3$; therefore at $x \gg 3$ the use of Maxwell-Boltzmann statistics becomes justifiable. If $x \ll 3$, then the equilibrium distribution for fermions and bosons may be written as $Y_{EQ}^{(\pm 1)}(x) = Y_{EQ}^{(0)} w^{(\pm 1)}(x)$, where $w^{(\pm 1)}(x)$ is some weight function. By fitting[4] the ratios of $Y_{EQ}^{(\eta)}(x)$ for different η, the weight function can be expressed by

$$w^{(\eta)}(x) = \begin{cases} \left\{ a^2 \left[\frac{2}{3\zeta(3)} - \frac{1}{2} \right] x^2 K_2(ax) + 1 \right\}^{-1} \text{ with } a = 0.10809\,, & \text{for } \eta = +1\,, \\ \left\{ 1 - \left[\frac{7 - 6\zeta(3)}{-4 + 3\zeta(3)} e^{-x} + 1 \right] \left[\frac{1}{w^{(-1)}(x)} - 1 \right] \right\}^{-1}\,, & \text{for } \eta = -1\,. \end{cases} \tag{4.7}$$

Using the approximate analytic functions (4.7) instead of the implicit (4.6) will reduce the numerical computing time of the Boltzmann equation. The high temperature limit is independent of the temperature:

$$\lim_{x \to 0} w^{(\eta)}(x) = \begin{Bmatrix} \frac{3\zeta(3)}{2} & \text{for } \eta = +1 \\ 2\zeta(3) & \text{for } \eta = -1 \end{Bmatrix} \quad \Rightarrow \quad \lim_{x \to 0} Y_{EQ}^{(\eta)}(x) = \frac{g}{2} \times \begin{Bmatrix} \frac{3}{4} & \text{for } \eta = +1 \\ 1 & \text{for } \eta = -1 \end{Bmatrix}.$$

[4]It turned out that the function $\frac{Y_{EQ}^{(0)}(x)}{Y_{EQ}^{(1)}(x)} - 1$ fits to function $ax^2 K_2(bx)$ where one of the constants can be fixed by the asymptotic value of $Y_{EQ}^{(1)}(0)$, whereas the function $1 - \frac{Y_{EQ}^{(0)}(x)}{Y_{EQ}^{(-1)}(x)}$ fits to Ce^{-x}, where C is determined by the asymptotic values of (4.6) at 0: $C = \frac{1 - \zeta(3)^{-1}}{4/3\zeta(3)^{-1} - 1} - 1$.

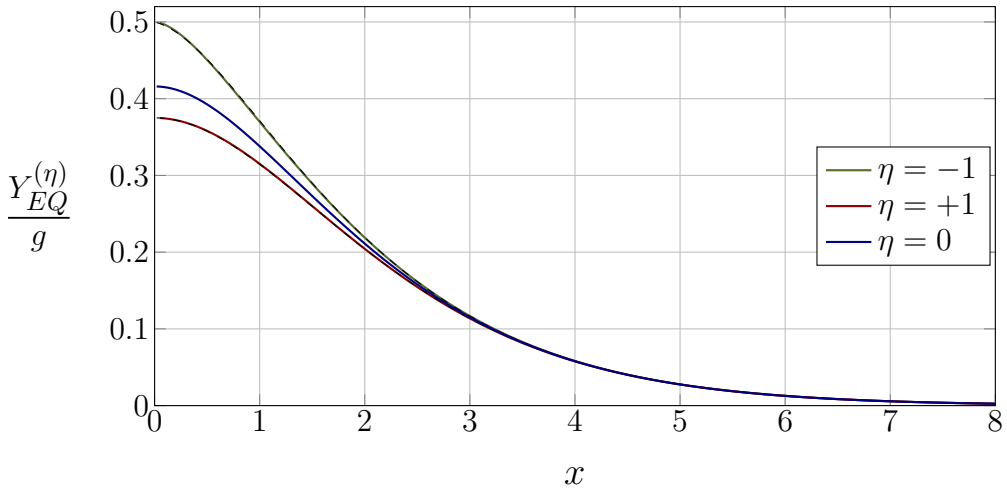

Figure 10: Equilibrium number density, $Y_{EQ}^{(\eta)}(x)$ for fermions (red) and bosons (green). If the temperature is low enough, the number density reduces to $Y_{EQ}(x) \equiv Y_{EQ}^{(0)}(x) = \frac{g}{4\zeta(3)} x^2 K_2(x)$ (blue). Approximations with the weight functions are in dashed line (but not very visible).

4.2. Freeze-in, freeze-out and the relic abundance

Freeze-out arises from the inability of the interactions to keep the particle(s) in chemical equilibrium with the plasma due to the expansion of the Universe (and decreasing temperature), thus leaving a constant abundance of the particles relative to that of the photons. There are essentially three regimes of the freeze-out, which depend on the dimensionless freeze-out temperature, $x_F \equiv \frac{m}{T_F}$, where T_F is temperature of the particle at the freeze-out: relativistic ($x_F \ll 3$), semi-relativistic ($x_F \sim 3$) and non-relativistic ($x_F \gg 3$). Depending on the initial abundance of the particles in equilibrium with the thermal plasma, the number density, Y, should follow the equilibrium number density until the freeze-out point, after which it departs from the equilibrium and remains approximately constant (assuming no future entropy production). In other words, the interactions $\gamma\gamma \leftrightarrow$ MCPs maintains the equilibrium until $\gamma\gamma \rightarrow$ MCPs stops around x_F. The abundance continues to fall due to MCPs $\rightarrow \gamma\gamma$ until there are too few MCPs left to annihilate into a pair of photons, thus leaving a final abundance. Stronger interactions will lead to a smaller final abundance, and in the absence of freeze-out there would be no particles left today since the equilibrium abundance goes exponentially to zero.

For the freeze-out to occur the particles must therefore be initially coupled to the thermal bath. If the initial abundance is smaller than that of equilibrium (due to inflation or some other mechanism) and the strength of producing interactions is feeble, the particles might never attain the equilibrium [32]. They are still produced due to the interactions with the thermal bath until their abundance reaches a constant yield around $x_F \sim \mathcal{O}(1)$ – they „freeze-in". Stronger interactions will lead to a higher yield until the equilibrium abundance is reached, which in turn is followed by the freeze-out. With the initial condition $Y(x_r) < Y_{EQ}(x_r)$ the theoretical maximum level of relic abundance is determined by the cross-over point of the two regimes.

Although there's no general closed-form expression for thermally averaged cross-section (besides the fact that the resulting differential equation, known as Riccati equation, also has no general solutions), the extreme cases are known to have good analytical approximations. In ultrarelativistic case the final relic abundance of the particles (initially in equilibrium) depends only on the d.o.f. of the particles [33]:

$$Y_0 = Y_{EQ}(x_F) = \frac{1}{2} \times \begin{cases} g & \text{(for bosons)} \\ \frac{3}{4}g & \text{(for fermions)} \end{cases} .$$

However, if the freeze-out temperature is large the thermally averaged cross-section can be approximated with its s- and p-wave solutions[5] or, equivalently, in Taylor series of x^{-1} because $\beta \propto x^{-\frac{1}{2}}$ [33][6]. The low-velocity expansion (β around 0) in (4.2) can be carried out in terms of y around $y_0 = 1$ instead,

$$\sigma(\beta)\Big|_{\beta\to\sqrt{1-y^{-1}}} = \sigma(4m^2 y) = \sum_{n=0}^{\infty} \sigma_n^{(y)} (y-1)^{n+\frac{1}{2}} =$$
$$= \begin{cases} \frac{1}{6}\sqrt{y-1} - \frac{17}{96}(y-1)^{\frac{3}{2}} + \frac{721}{1920}(y-1)^{\frac{5}{2}} + \mathcal{O}\left((y-1)^{\frac{7}{2}}\right) & \text{spin-0} \\ \frac{1}{8}\sqrt{y-1} + \frac{1}{16}(y-1)^{\frac{3}{2}} - \frac{141}{320}(y-1)^{\frac{5}{2}} + \mathcal{O}\left((y-1)^{\frac{7}{2}}\right) & \text{spin-}\frac{1}{2} \\ \frac{19}{16}\sqrt{y-1} - \frac{33}{32}(y-1)^{\frac{3}{2}} + \frac{961}{640}(y-1)^{\frac{5}{2}} + \mathcal{O}\left((y-1)^{\frac{7}{2}}\right) & \text{spin-1} \end{cases} ,$$

[5] s- and p-wave modes of a thermally averaged cross-section are β^0 and β^2 terms in its low-velocity expansion.

[6] According to kinetic theory of gases, the (mean) velocity of particles is proportional to $\sqrt{\frac{T}{m}}$. The relationship still holds in current context as $\beta \approx 0$.

which enables to calculate an easily integrable expression

$$\begin{aligned}\langle\sigma v\rangle_f &= \frac{4x}{K_2^2(x)}\sum_{n=0}^{\infty}\sigma_n^{(y)}\int_1^{\infty}\sqrt{y}(y-1)^{n+\frac{1}{2}}K_1(2x\sqrt{y})\ \mathrm{d}y = \\ &= \frac{4}{K_2^2(x)}\sum_{n=0}^{\infty}\sigma_n^{(y)}x^{-n-\frac{1}{2}}\Gamma\left(n+\frac{3}{2}\right)K_{n+\frac{5}{2}}(2x) \approx \\ &\approx \frac{1}{\sqrt{\pi}}\left[\sigma_1^{(y)}x^{-1}+\left(\sigma_2^{(y)}-\frac{3\sigma_1^{(y)}}{4}\right)x^{-2}+\left(\frac{45\sigma_1^{(y)}}{32}+\frac{5\sigma_2^{(y)}}{4}+\sigma_3^{(y)}\right)x^{-3}\right]+\mathcal{O}(x^{-4}) \equiv \\ &\equiv \sum_{n=1}^{\infty}(\sigma v)_n x^{-n}\,.\end{aligned}$$

If $x \gg 3$ then $Y_{EQ}(x) \ll Y(x)$ and the equilibrium number density can be neglected altogether in (4.3). In that case the relic density has the following approximation:

$$Y_0 = \left(Y(x_F)^{-1}+\int_{x_F}^{x_0}\lambda\ \langle\sigma v\rangle_f(x)x^{-2}\ \mathrm{d}x\right)^{-1}. \tag{4.8}$$

It can already be seen that the abundance today is inversely proportional to the (thermally averaged) cross-section – if some particles annihilate with a higher probability than others, it is to be expected that their abundance in current cosmological epoch be smaller.

The condition for the freeze-out temperature x_F is $Y(x_F) = cY_{EQ}(x)$, where $c = \mathcal{O}(1)$ is chosen by hand. A rough estimate can be obtained by plugging the equality into (4.3) and assuming that $Y_{EQ}^{(\eta)}(x) \simeq Y_{EQ}(x) \approx ax^{\frac{3}{2}}e^{-x}$ with $a = \sqrt{\frac{\pi}{8}}\frac{g}{2\zeta(3)}$ [33]:

$$e^{x_F} \simeq (c^2-1)a(\sigma v)_1\lambda x_F^{-\frac{1}{2}}$$

The equation can be solved with the Lambert W-function:

$$x_F = \frac{1}{2}W(2r^2) \quad \text{where} \quad r = (c^2-1)a(\sigma v)_1\lambda\,. \tag{4.9}$$

The density of MCPs (or any particle, for that matter) is given by $\Omega_{\mathrm{MCP}} = \frac{\rho_{\mathrm{MCP}}}{\rho_{\mathrm{cr}}}$, where $\rho_{\mathrm{cr}} = \frac{3H^2}{8\pi G}$ is the critical density of the Universe [34, p. 337]. The physical MCP density today can be expressed by

$$\Omega_{\mathrm{MCP}}h^2 = \frac{\rho_{\mathrm{MCP},0}}{\rho_{\mathrm{cr},0}}h^2 = \frac{8\pi G}{3H_0^2}h^2 m s_0 Y_0\,, \tag{4.10}$$

where $H_0 = 67.74(46)\,\mathrm{km\,s^{-1}\,Mpc^{-1}}$ is the Hubble rate today, h is reduced Hubble constant (defined in such a way that $H_0 = h\,100\mathrm{km\,s^{-1}\,Mpc^{-1}}$) and $s_0 = 2900\ \mathrm{cm^{-3}}$ is the entropy density today [3, p. 122][35, p. 31][36, p. 15]. The expression assumes that the Universe

expands isentropically; if the entropy should increase by some factor, then the number density (and hence the physical abundance) should decrease by the same factor.

The latest Planck data suggest that the physical dark matter density is $\Omega_c h^2 = 0.1188(10)$ [35, p. 31]. Assuming that the density of MCPs is smaller than or equal to that of dark matter, a direct bound on the charge and mass can be set. A very rough estimate on Y_0 can be obtained by treating g_* as a constant and integrating the Boltzmann equation from zero to infinity:

$$Y_0 = \left(\frac{1}{cY_{EQ}(x_F)} + \lambda \sum_{n=1}^{\infty} (\sigma v)_n \frac{x_F^{n+1}}{n+1} \right)^{-1} ,$$

which then leads to the constraint (see (4.4) for the definition of α)

$$\frac{1}{m} \left(\frac{1}{cY_{EQ}(x_F)} + \frac{q^4}{m} \alpha \sum_{n=1}^{\infty} (\sigma v)_n \frac{x_F^{n+1}}{n+1} \right) \geqslant \frac{8\pi G h^2 s_0}{3H_0^2(\Omega_c h^2)} . \tag{4.11}$$

4.3. Direct numerical solution

A direct numerical approach to the problem (4.3) has been carried out for a large range of λ since it's easier to fit the curves $Y_0(\lambda)$ and then impose the constraint $\Omega_{\text{MCP}} < \Omega_c$. Firstly, a piecewise continuous approximation to $\langle \sigma v \rangle_f$ is needed. The region $x \lesseqgtr \mathcal{O}(10)$ fits to the function ax^b; the region in between is approximated by a piecewise function of quadratic polynomials[7]. The result, depicted in fig. 11, shows normalized thermally averaged cross-section for MCPs of all spins. Interestingly, $\langle \sigma v \rangle_f$ for spin-1 MCPs stays constant until $x \sim 1$.

The next step is to plug the obtained functions into the Boltzmann equation and solve it numerically[8] for a range of λ with a finite initial condition for x. The table in fig. 12 shows the precise ranges and initial conditions for each spin. Unfortunately, the Boltzmann equation with no initial (particularly spin-1) MCP abundance is stiff in the sense that the solution is rapidly changing which causes numerical instabilities (e.g. infinitely small step size). The problem can be alleviated by choosing larger x in the initial condition and reducing the precision sought.

[7] Mathematica's NonlinearModelFit has been used, which defaulted to Levenberg-Marquardt method.

[8] Mathematica's default NDSolve has been used with the options AccuracyGoal→10, PrecisionGoal→10 and MaxSteps→$2{\cdot}10^4$.

As can be seen from fig. 12, freeze-in occurs when the interaction strength ($\sim \lambda$) is very small. The freeze-in of vector MCPs looks distinct compared to that of other spins – the abundance of feebly interacting MCPs never tries to reach the equilibrium –, and might be a consequence of ultraviolet freeze-in [37]. Subplot 4.13(c) also shows that the relic density depends inversely on the initial condition x_r in the freeze-in regime.

Relations between the final relic abundance Y_0, parameter λ and the freeze-out temperature (x_F) can be drawn from the numerical data. The condition used to find the freeze-out temperature reads

$$\left| \frac{Y(x_F)}{Y_{EQ}(x)} - c \right| < \epsilon \quad \text{with} \quad c = 10 \quad \text{and} \quad \epsilon = 10^{-5} \,.$$

Although the definition above in the context of freeze-in isn't proper, the relation is still applied to it for illustrative purposes. The plots of all relations are given in figure 13. The results of spin-1 MCPs are particularly interesting since the final relic density remains almost maximum for $\lambda = 10^{-4} \ldots 1$. Subplot 4.13(d) shows that if the freeze-out temperature is large enough (or equivalently, if the interaction is strong enough), the contribution of thermally averaged cross-section (in (4.8)) becomes important.

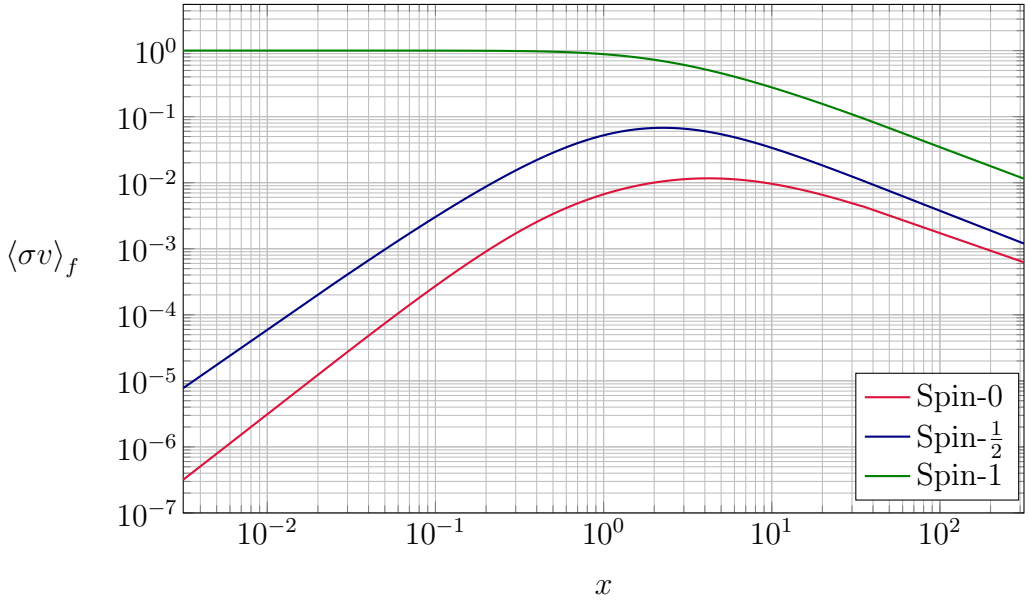

Figure 11: Normalized thermally averaged cross-section (dimensionless) (4.2). It should be noted that the interaction rate is proportional to the thermally averaged cross-section: $\Gamma = \langle \sigma v \rangle \, n_\gamma$. Thus, if the temperature of the plasma decreases until m, the interaction rate starts falling exponentially.

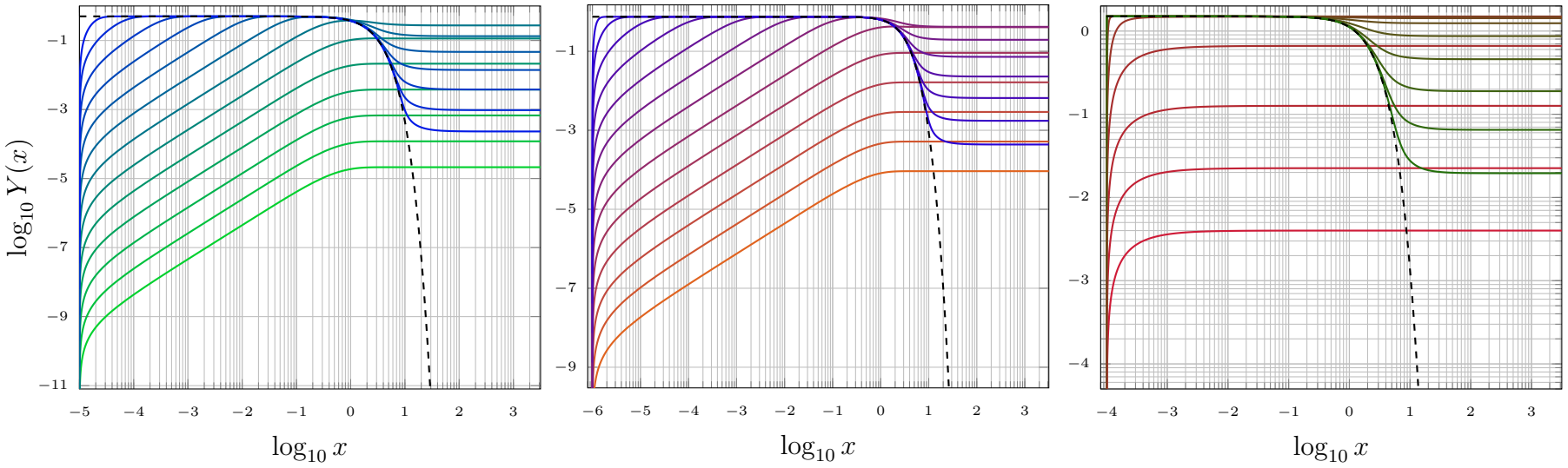

(a) Spin-0 (b) Spin-$\frac{1}{2}$ (c) Spin-1

Figure 12: The number density $Y(x)$ for MCPs of all spins. The dashed lines represent the equilibrium number density, $Y_{EQ}^{(\eta)}(x)$. The solutions are found for a wide range of λ with logarithmically uniform step $\Delta \log_{10} \lambda = 0.75$ (see table below). If λ is small enough, the freeze-in occurs and the number density remains on a constant level around $x \sim \mathcal{O}(1)$. On the other hand, if λ is large enough, the number density follows the equilibrium path for a while and then freezes out. The turning point, $\lambda_{\rm tp}$, is where the final relic density, Y_0, reaches the maximum.

	spin-0	spin-$\frac{1}{2}$	spin-1
Range of λ	10^{-2} (green) $\ldots 10^{7}$ (blue)	$10^{-2.75}$ (orange) $\ldots 10^{6.25}$ (blue)	$10^{-6.5}$ (red) $\ldots 10^{3.25}$ (green)
Initial condition $Y(x_r) = 0$	$x_r = 10^{-5}$	$x_r = 10^{-6}$	$x_r = 10^{-4}$
$\max Y_0(\lambda) = \max \lim_{x\to\infty} Y(\lambda; x)$ (% of $\max Y_{EQ}^{(\eta)}(x)$)	0.276 (55.2%)	0.513 (68.4%)	1.49 (99.6%)
$\lambda_{\rm tp} = \arg\max Y_0(\lambda)$	$\lambda_{\rm tp} = 154.7$	$\lambda_{\rm tp} = 12.70$	$\lambda_{\rm tp} = 1.660 \cdot 10^{-3}$

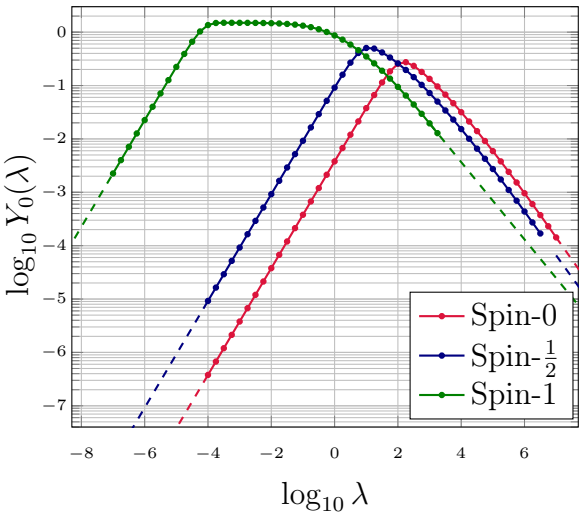

(a) Final relic density vs λ

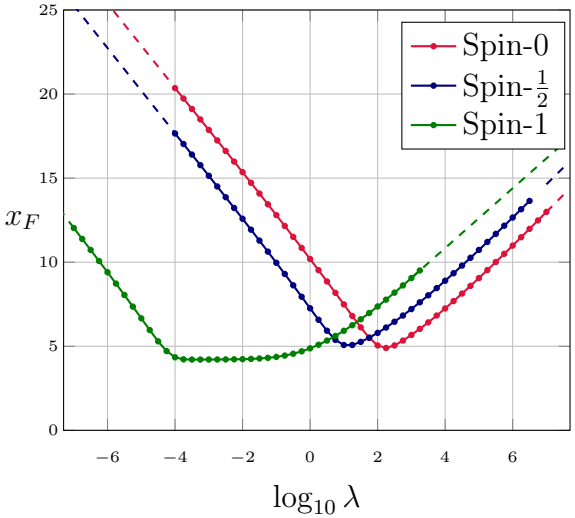

(b) Freeze-out temperature vs λ

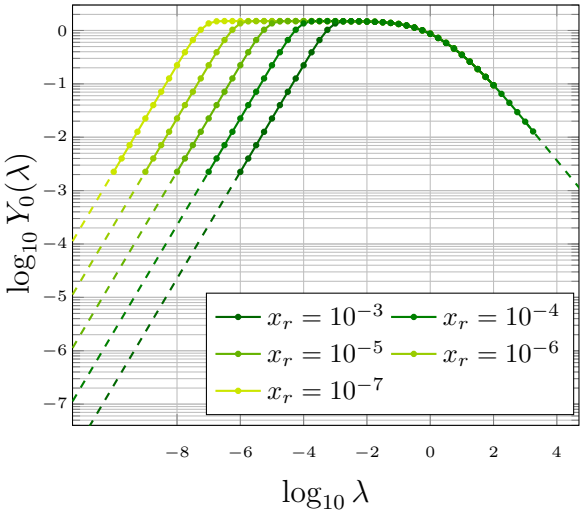

(c) Final relic density vs λ for spin-1 MCPs with different initial conditions x_r

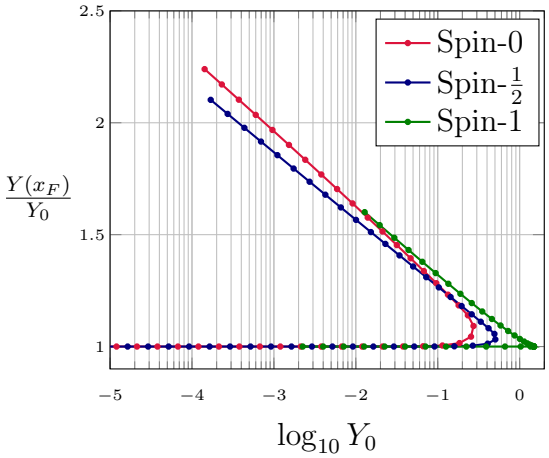

(d) Yield at freeze-out vs final relic density

Figure 13: The dots are the solutions to the Boltzmann equation for each λ. The dashed lines are extrapolated from the interpolation curve obtained for specific range of λ (small or large w.r.t the turning point λ_{tp}). Step of λ here is $\Delta\lambda = 10^{0.25}$. The plots 4.13(a), 4.13(b) and 4.13(d) use initial conditions specified in the table of fig. 12.

4.4. Constraints on mass and charge

Substitution of the constants in (4.10) with their values results in the constraint

$$mY_0 \leqslant 0.431672 \text{ eV} \equiv \kappa \,. \tag{4.12}$$

By knowing the maximum final relic density for each spin (see table in fig. 12), we can estimate the minimal particle masses affected by the constraint (4.12), which are

$$\begin{aligned} m_{\text{min}}^{(0)} &= 1.578 \text{ eV} \quad \text{(spin-0)}\,, \\ m_{\text{min}}^{(1/2)} &= 0.854 \text{ eV} \quad \left(\text{spin-}\tfrac{1}{2}\right), \\ m_{\text{min}}^{(1)} &= 0.288 \text{ eV} \quad \text{(spin-1)}\,. \end{aligned} \tag{4.13}$$

According to our model, the MCPs lighter than m_{min} cannot make up all DM since their abundance would be always smaller than that of DM.

Interpolation of the curve 4.13(a) in the freeze-in/out regime helps to set bounds in the (q, m) parameter space. By fixing the actual MCP yield to Y_0^c we find two corresponding possible values of λ: one from the freeze-in mechanism (λ_{FI}^c) and the other from the freeze-out (λ_{FO}^c). The yield Y_0 in the freeze-in and freeze-out regimes can be approximated by $Y_0^{FI}(\lambda) = a\lambda$ and $Y_0^{FO}(\lambda) = a\lambda^{-b}$ (with both constants a, $b > 0$), respectively. However, as already mentioned, the relic density in case of spin-1 MCPs in freeze-in regime depends on the inverse of the reheating temperature due to the initial condition $Y(x_r) = 0$, which leads to the approximation

$$Y_0^{FI} = a\frac{T_{RH}}{m}\lambda \,. \quad \text{(spin-1)} \tag{4.14}$$

The freeze-in sets a constant (log-linear in case of vector MCPs) upper bound on their charge for the mass region larger than m_{min} since

$$q \leqslant \sqrt[4]{\frac{\kappa}{a\alpha}} \quad \text{(spin-0, spin-}1/2\text{)}\,, \qquad q \leqslant \sqrt[4]{\frac{\kappa m}{a\alpha T_{RH}}} \quad \text{(spin-1)}\,. \tag{4.15}$$

The final yield in freeze-out, Y_0^{FO}, becomes larger with increasing mass, thus leading to a lower bound on q for the same mass range:

$$ma\left(\alpha\frac{q^4}{m}\right)^{-b} \leqslant \kappa \quad \Rightarrow \quad q \geqslant \sqrt[4b]{\frac{am}{\kappa}\left(\frac{m}{\alpha}\right)^b}\,. \tag{4.16}$$

Table 1 sums up the results from interpolation. The final result is the exclusion plot in (q, m) parameter space depicted in fig. 14.

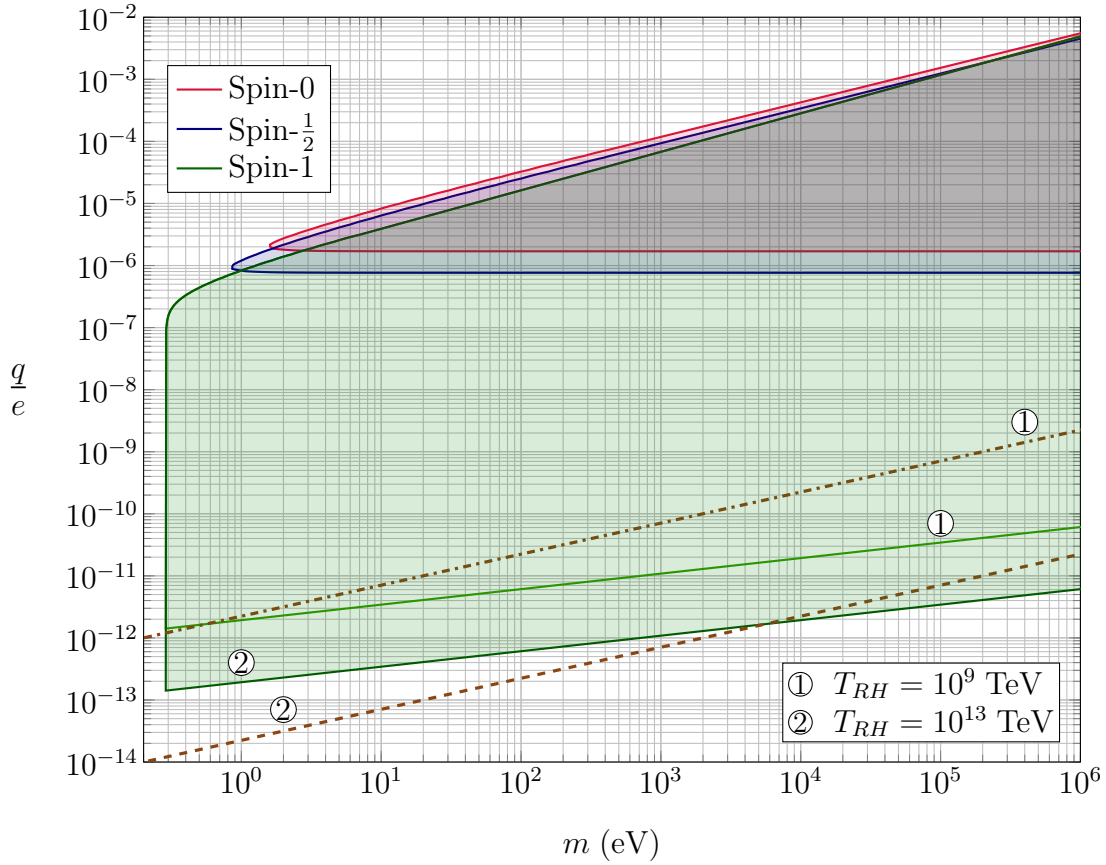

Figure 14: Charge vs mass exclusion plot for MCPs. The filled area shows the values in (q, m) parameter space excluded by the observed abundance of DM. The upper bounds on vector MCPs are found for $T_{RH} = 10^9$ TeV and $T_{RH} = 10^{13}$ TeV. Corresponding dash-dotted and dashed lines represent the lower limit on charge above which the production and annihilation of MCPs (via freeze-in) dominate (see (4.17)).

Regime	Parameter	Spin-0	Spin-$\frac{1}{2}$	Spin-1
Freeze-in, (4.15)	a	3.789×10^{-3}	9.219×10^{-2}	2.249
Freeze-out, (4.16)	a	74.58	27.98	2.128
	b	0.815	0.801	0.676

Table 1: Results of the interpolation based on fig. 4.13(a).

Maximum relativistic d.o.f., $g_* = 106.75$, allowed by the Standard Model has been used in the above plot. Using present day's $g_* = 3.35$ instead would lead to a $\left(\frac{106.75}{3.35}\right)^{\frac{1}{8}} \approx 1.5$ reduction of the upper and lower bound on q.

The upper bounds on the charge of scalar and fermion MCPs are $q_0 = 1.69 \times 10^{-6}e$ and $q_{1/2} = 7.63 \times 10^{-7}e$. Unfortunately, the precise value of the reheating temperature has still remained unknown, which greatly affects the upper bound of vector MCPs. The currently allowed range for the reheating temperature is 10 MeV $\lesssim T_{RH} \lesssim 10^{13}$ TeV as bounded from BBN and inflation [38].

The upper bound on vector MCPs (4.14) is not universal for any mass range. If new interaction involving MCPs were to add a $\sim q^2$ term to their cross-section of production, the inequality (4.15) would become

$$\alpha \left(a q^4 x_r^{-1} + a' q^2 \right) \leqslant \kappa \,, \tag{4.17}$$

where a' depends on the particular model considered. The upper bounds found for vector MCPs are valid only in the region where $q \geqslant \frac{a'm}{aT_{RH}}$, or equivalently, up to some mass: $m \leqslant q^2 T_{RH} a/a'$. If the MCPs are too massive or have too tiny charge, their production via photon annihilation is suppressed and the upper limits on MCPs cannot be set in our model. In a yet unpublished work by the supervisors of this thesis they concluded that the constant a' for $SU(2)$ model of MCPs is $a' = 4 \times 10^{-3}$. The corresponding lower limits on charge above which the photon interactions prevail are also depicted in fig. 14. If the reheating temperature is less than $\sim 10^9$ TeV, then no upper limits on the charge of MCPs can be set.

5. Summary

The current stance in modern physics suggests that about a quarter of the Universe comprises dark matter (DM), the exact nature of which still remains unknown. When proposing a new kind of particle as a DM candidate it is necessary to make sure that its physical characteristics are compatible with the currently established paradigms in cosmology and particle physics. One of the proposed DM candidates is a particle that has a tiny electric charge and is thereby referred to as the millicharged particle (MCP). This type of particle, however, cannot have arbitrary charge and mass to make up all the observed DM abundance, because it would contradict the outcome of certain experiments and observations.

The thesis focused on a simplified theory of MCPs for spins 0, $1/2$ and 1 (with the emphasis on vector MCPs), in which only the interactions with photons are considered. The Lagrangian of vector MCPs interacting with the photons is described in chapter 3, along with the calculation of the (polarized) cross-section for the process $\gamma\gamma \to$ MCPs. The annihilation and production of MCPs in the early Universe kead to an observable abundance of these particles as described by the Boltzmann equation that governs its evolution. By solving the Boltzmann equation for MCPs as well as assuming that their initial abundance after inflation is very small and the current abundance is less than or equal to that of DM, we derived the direct bound on MCP mass and charge shown in equations (4.13), (4.15) and (4.16).

According to our results, the freeze-in of scalar and fermion MCPs sets a constant upper limit on their charge, $\lesssim 10^{-6}e$, in the mass range 1 eV $\lesssim$. Differently, the relic abundance of vector MCPs created in the same fashion depends log-linearly on their mass and on the inverse of the reheating temperature of the Universe. Since the allowed values of the latter span orders of magnitude, it is not possible to cast a precise upper bound on the charge of vector MCPs. Furthermore, it might be the case that no upper limit on vector MCPs can be set in our approximation if the actual value of the reheating temperature is too small. In the case of production via freeze-out, on the other hand, we obtained a mass- and spin-dependent lower limit on the charge of MCP as described in section 4.4. The constraints that our methodology casts on the masses and charges of

MCPs are summarized in fig. 14.

As a final note, I would like to thank my supervisors Hardi Veermäe, who provided (further) insight into the topic that proved to be invaluable, and Luca Marzola, who helped me out on conceptual matters.

Bibliography

[1]B. Holdom, "Two U(1)'s and ε charge shifts", Physics Letters B **166**, 196–198 (1986).

[2]J. Jaeckel, "Photons as a Probe of Minicharged Particles", (2007).

[3]E. Kolb and M. Turner, *The Early Universe* (Westview Press, 1994).

[4]J. Redondo, "Can the PVLAS particle be compatible with the astrophysical bounds?", (2008).

[5]J. Jaeckel and A. Ringwald, "The Low-Energy Frontier of Particle Physics", (2010).

[6]S. Davidson, S. Hannestad, and G. Raffelt, "Updated bounds on milli-charged particles", Journal of High Energy Physics **2000** (2000) 10.1088/1126-6708/2000/05/003.

[7]Z. Berezhiani, A. Dolgov, and I. Tkachev, "BBN with light dark matter", J. Cosmol. Astropart. Phys. **2013**, 010–010 (2013).

[8]S. Dodelson, *Modern Cosmology* (Academic Press, 2003).

[9]D. J. Fixsen, "The Temperature of the Cosmic Microwave Background", The Astrophysical Journal **707**, 916–920 (2009).

[10]A. Melchiorri, A. Polosa, and A. Strumia, "New bounds on millicharged particles from cosmology", Physics Letters B **650**, 416–420 (2007).

[11]C Burrage, J Jaeckel, J Redondo, and A Ringwald, "Late time CMB anisotropies constrain mini-charged particles", J. Cosmol. Astropart. Phys. **2009**, 002–002 (2009).

[12]A. D. Dolgov, S. L. Dubovsky, G. I. Rubtsov, and I. I. Tkachev, "Constraints on millicharged particles from Planck", Phys. Rev. D **88,** 117701 (2013).

[13]J. Jaeckel, M. Jankowiak, and M. Spannowsky, "LHC probes the hidden sector", Physics of the Dark Universe **2**, 111–117 (2013).

[14]A. De Angelis, O. Mansutti, M. Persic, and M. Roncadelli, "Photon propagation and the very high energy γ-ray spectra of blazars: how transparent is the Universe?", Monthly Notices of the Royal Astronomical Society: Letters **394**, L21–L25 (2009).

[15]H Gies, J Jaeckel, and A Ringwald, "Accelerator cavities as a probe of millicharged particles", Europhysics Letters (EPL) **76**, 794–800 (2006).

[16]A. Prinz, R. Baggs, J. Ballam, S. Ecklund, C. Fertig, J. Jaros, K. Kase, A. Kulikov, W. Langeveld, R. Leonard, and et al., "Search for Millicharged Particles at SLAC", Physical Review Letters **81**, 1175–1178 (1998).

[17]M. Bregant, G. Cantatore, S. Carusotto, R. Cimino, F. Della Valle, G. Di Domenico, U. Gastaldi, M. Karuza, V. Lozza, E. Milotti, and et al., "Limits on low energy photon-photon scattering from an experiment on magnetic vacuum birefringence", Phys. Rev. D **78** (2008) 10.1103/physrevd.78.032006.

[18]M. Ahlers, H. Gies, J. Jaeckel, and A. Ringwald, "Particle interpretation of the PVLAS data: Neutral versus charged particles", Phys. Rev. D **75** (2007) 10.1103/physrevd.75.035011.

[19]E. Zavattini, G. Zavattini, G. Ruoso, G. Raiteri, E. Polacco, E. Milotti, V. Lozza, M. Karuza, U. Gastaldi, G. Di Domenico, and et al., "New PVLAS results and limits on magnetically induced optical rotation and ellipticity in vacuum", Phys. Rev. D **77** (2008) 10.1103/physrevd.77.032006.

[20]B. Lautrup and E. de Rafael, "Calculation of the Sixth-Order Contribution from the Fourth-Order Vacuum Polarization to the Difference of the Anomalous Magnetic Moments of Muon and Electron", Phys. Rev. **174**, 1835–1842 (1968).

[21]M. Gluck, S. Rakshit, and E. Reya, "Lamb shift contribution of very light charged particles", Phys. Rev. D **76** (2007) 10.1103/physrevd.76.091701.

[22]D. Angom, K. Bhattacharya, and S. D. Rindani, "Decay of Spin-One Particle into Two Photons in Presence of Uniform External Magnetic Field", International Journal of Modern Physics A **22**, 707–720 (2007).

[23]A. Czarnecki, "Positronium properties", Acta Phys.Polon. **B30**, 3837–3847 (1999).

[24]A. Badertscher, P. Crivelli, W. Fetscher, U. Gendotti, S. N. Gninenko, V. Postoev, A. Rubbia, V. Samoylenko, and D. Sillou, "Improved limit on invisible decays of positronium", Phys. Rev. D **75** (2007) 10.1103/physrevd.75.032004.

[25]S. Ferrara, M. Porrati, and V. Telegdi, "g=2 as the natural value of the tree-level gyromagnetic ratio of elementary particles", Phys. Rev. D **46**, 3529–3537 (1992).

[26]M. E. Peskin and D. V. Schroeder, *An Introduction To Quantum Field Theory* (Westview Press, 1995).

[27]S. L. Adler, S. Mandelstam, S. Weinberg, and W. Zimmermann, *Lectures On Elementary Particles and Quantum Field Theory (Volume 1)*, edited by S. Deser, M. Grisaru, and H. Pendleton (The MIT Press, 1971).

[28]B. R. Holstein, "How large is the „natural" magnetic moment?", Am. J. Phys. **74**, 1104 (2006).

[29]F. Mandl and G. Shaw, *Quantum field theory* (John Wiley & Sons, 2010).

[30]V. Chiochia, G. Dissertori, and T. Gehrmann, *Phenomenology of Particle Physics I*, Lecture notes, June 2014.

[31]P. Gondolo and G. Gelmini, "Cosmic abundances of stable particles: Improved analysis", Nuclear Physics B **360**, 145–179 (1991).

[32]L. J. Hall, K. Jedamzik, J. March-Russell, and S. M. West, "Freeze-in production of FIMP dark matter", J. High Energ. Phys. **2010** (2010) 10.1007/jhep03(2010)080.

[33]R. J. Scherrer and M. S. Turner, "On the relic, cosmic abundance of stable, weakly interacting massive particles", Phys. Rev. D **33**, 1585–1589 (1986).

[34]S. Carroll, *Spacetime and Geometry: An Introduction to General Relativity* (Addison-Wesley, 2003).

[35]Planck Collaboration, "Planck 2015 results. XIII. Cosmological parameters", arXiv:1502.01589 (2015).

[36]K. Schmitz, *The B-L Phase Transition: Implications for Cosmology and Neutrinos* (Springer Science & Business Media, 2013).

[37]F. Elahi, C. Kolda, and J. Unwin, "UltraViolet freeze-in", J. High Energ. Phys. **2015** (2015) 10.1007/jhep03(2015)048.

[38]J. Martin and C. Ringeval, "First CMB constraints on the inflationary reheating temperature", Phys. Rev. D **82** (2010) 10.1103/physrevd.82.023511.

[39]C. L. Lewis, "Explicit gauge covariant Euler-lagrange equation", Am. J. Phys. **77**, 839 (2009).

Piirangud millilaetud tumeaine massile ja laengule

Karl Ehatäht

Kokkuvõte

Millilaetud osakesed (MLOd) ehk osakesed, mis omavad väga väikset elektrilaengut, ilmuvad mitmetes fundamentaalfüüsika ühendteooriates ning neid võib käsitleda kui üht võimalikku tumeaine kanditaati. Antud töö uuris lihtsustatud millilaetud osakeste mudelit, milles kõik ülejäänud interaktsioonid osakestega peale footonite on ignoreeritud. Erilist tähelepanu on pööratud vektor-bosonitele, kuna laetud vektor-bosonite ja neist moodustatud tumeaine fenomenoloogiat pole seni uuritud (jättes kõrvale osakese spinnist sõltumatud analüüsid).

Eeldus, et tänane millilaetud osakeste kogus on väiksem või võrdne vaadeldud tumeaine omaga, seab piirangud MLOde laengule ja massile. Käesolevas töös arvutati tänane MLOde hulk sõltuvalt nende massist ja laengust Boltzmanni võrrandi abil, mille sisendiks on protsessi $\gamma\gamma \to$ MLOd mõjuristlõige (arvutatud peatükis 3). Boltzmanni võrrandi kontekstis on vaadeldud juhtu, kus MLOde algne numbriline tihedus on väga väike vahetult pärast inflatsiooni. Antud töös uuritakse lisaks MLOde väljakülmumisele (eraldumisele osakeste plasmast) ka teist efekti – sissekülmumist.

Väljakülmumine võimaldas määrata massist ja spinnist sõltuva alumise tõkke osakeste massile suuremad kui ~ 1 eV. Sissekülmumine seevastu andis osakese massist sõltumatu konstantse ülemise tõkke millilaetud skalaarse bosoni ja fermioni laengule, $q \lesssim 10^{-6}e$. Osutus, et sama piirang millilaetud vektor-bosonile antud lähenduse kehtivuspiirkonnas kas sootuks puudub või sõltub pöördvõrdeliselt Universumi eelsoojenemistemperatuurist (*reheating temperature*), mille täpset väärtust pole seni kindlaks tehtud. Massi ja laengu väärtuste hulka, mis antud mudelis välistavad MLOde esinemise, on kokku võetud graafikul 14.

A. Process $\gamma\gamma \to$ MCPs – calculations

A.1. Vector boson case

A.1.1. Lagrangian for MCP

Here we present the explicit calculations omitted in 3.1 and 3.2 for the sake of readability.

Definitions

- Källen function: $\lambda(x,\, y,\, z) = x^2 + y^2 + z^2 - 2xy - 2xz - 2yz\,.$ (A.1)
- Mandelstam variables (a, b initial particles, 1, 2 final particles)

$$\begin{gathered} s = (p_a + p_b)^2 = (p_1 + p_2)^2, \quad t = (p_a - p_1)^2 = (p_b - p_2)^2, \\ u = (p_a - p_2)^2 = (p_b - p_1)^2\,. \end{gathered} \tag{A.2}$$

  $\sqrt{s}$ is also the c.m. energy.

- Integration limits of (3.9): $t_{\substack{\min,\\ \max}} = m^2 - \frac{1}{2}\left(s \pm \sqrt{\lambda(s,\, m^2,\, m^2)}\right)\,.$ (A.3)

Proof that $W^{\mu\nu}\widetilde{W}^{\dagger}_{\mu\nu} \propto \widetilde{F}^{\mu\nu}W^{\dagger}_{\mu}W_{\nu}$

$$\begin{aligned} W^{\mu\nu}\widetilde{W}^{\dagger}_{\mu\nu} &= \epsilon^{\mu\nu\rho\sigma}(D_\mu W_\nu - D_\nu W_\mu)(D_\rho W_\sigma - D_\sigma W_\rho)^\dagger = 4\epsilon^{\mu\nu\rho\sigma}(D_\mu W_\nu)(D^\dagger_\rho W^\dagger_\sigma) = \\ &= 4\epsilon^{\mu\nu\rho\sigma}\left[(\partial_\mu + iqA_\mu)W_\nu\right]\left[(\partial_\rho - iqA_\rho)W^\dagger_\sigma\right] = \\ &= 4\epsilon^{\mu\nu\rho\sigma}[(\partial_\mu W_\nu)(\partial_\rho W^\dagger_\sigma) - iqA_\rho W^\dagger_\sigma \partial_\mu W_\nu + iqA_\mu W_\nu \partial_\rho W^\dagger_\sigma + q^2 A_\mu W_\nu A_\rho W^\dagger_\sigma] = \\ &= \left[\epsilon^{\mu\nu\rho\sigma}\partial_\mu(W_\nu \partial_\rho W^\dagger_\sigma) = \epsilon^{\mu\nu\rho\sigma}(\partial_\mu W_\nu)(\partial_\rho W^\dagger_\sigma) + \epsilon^{\mu\nu\rho\sigma}W_\nu(\partial_\mu\partial_\rho W^\dagger_\sigma) \simeq 0\right] = \\ &= 4iq\epsilon^{\mu\nu\rho\sigma}(A_\mu W_\nu \partial_\rho W^\dagger_\sigma + A_\mu W^\dagger_\sigma \partial_\rho W_\nu) = 4iq\epsilon^{\mu\nu\rho\sigma}A_\mu\partial_\rho(W_\nu W^\dagger_\sigma) = \\ &= \left[\epsilon^{\mu\nu\rho\sigma}\partial_\rho(A_\mu W_\nu W^\dagger_\sigma) = \epsilon^{\mu\nu\rho\sigma}A_\mu\partial_\rho(W_\nu W^\dagger_\sigma) + \epsilon^{\mu\nu\rho\sigma}(\partial_\rho A_\mu)W_\nu W^\dagger_\sigma \simeq 0\right] = \\ &= -4iq\epsilon^{\mu\nu\rho\sigma}(\partial_\rho A_\mu)W_\nu W^\dagger_\sigma = 4iq\epsilon^{\mu\nu\rho\sigma}(\partial_\rho A_\sigma)W_\nu W^\dagger_\mu = \\ &= 2iq\epsilon^{\mu\nu\rho\sigma}(\partial_\rho A_\sigma - \partial_\sigma A_\rho)W_\nu W^\dagger_\mu = 2iq\widetilde{F}^{\mu\nu}W^\dagger_\mu W_\nu\,. \end{aligned}$$

The fourth and sixth lines show that adding a surface term to the Lagrangian does not change the underlying physics (i.e. equation of motion).

Equation of motion for MCPs

The equation of motion can be found through a gauge covariant version of the Euler-Lagrange equation [39],

$$D_\nu \left(\frac{\partial \mathcal{L}}{\partial (D_\nu^\dagger W_\mu^\dagger)} \right) - \frac{\partial \mathcal{L}}{\partial W_\mu^\dagger} = 0 \,.$$

Given that

$$\frac{\partial \mathcal{L}}{\partial (D_\rho^\dagger W_\sigma^\dagger)} = -\frac{1}{2} W^{\mu\nu} (\delta_\mu^\rho \delta_\nu^\sigma - \delta_\nu^\rho \delta_\mu^\sigma) + \xi g^{\mu\nu} \delta_\mu^\rho \delta_\nu^\sigma D_\alpha W^\alpha = -\frac{1}{2}(W^{\rho\sigma} - W^{\sigma\rho}) + \xi g^{\rho\sigma} D_\mu W^\mu =$$
$$= -W^{\rho\sigma} + \xi g^{\rho\sigma} D_\mu W^\mu \,,$$

$$\frac{\partial \mathcal{L}}{\partial W_\sigma^\dagger} = m^2 W^\mu \delta_\mu^\sigma + iq W_\nu \delta_\mu^\sigma (g_1 F^{\mu\nu} + g_2 \widetilde{F}^{\mu\nu}) = m^2 W^\sigma + iq W_\nu (g_1 F^{\sigma\nu} + g_2 \widetilde{F}^{\sigma\nu}) \,,$$

the equation of motion reads

$$D_\mu W^{\mu\nu} + m^2 W^\nu - \xi D^\nu D_\mu W^\mu - iq W_\mu (g_1 F^{\mu\nu} + g_2 \widetilde{F}^{\mu\nu}) = 0 \,. \tag{A.4}$$

Covariant derivative in the equation of motion

It can be shown that

$$D_\nu D_\mu W^{\mu\nu} = D_\nu D_\mu D^\mu W^\nu - D_\mu D_\nu D^\nu W^\mu - iq F_{\nu\mu} D^\nu W^\mu = iq F^{\mu\nu} D_\nu W_\mu = -\tfrac{iq}{2} F^{\mu\nu} W_{\mu\nu} \,,$$
$$D_\nu F^{\mu\nu} = (\partial_\nu + iq A_\nu) F^{\mu\nu} = -J^\mu + iq A_\nu F^{\mu\nu} \,,$$
$$D_\nu \widetilde{F}^{\mu\nu} = (\partial_\nu + iq A_\nu) \widetilde{F}^{\mu\nu} = iq A_\nu \widetilde{F}^{\mu\nu} \,,$$

which leads to

$$0 = -\frac{iq}{2} F^{\mu\nu} W_{\mu\nu} + m^2 D_\nu W^\nu - iq \, (D_\nu W_\mu) \left(g_1 F^{\mu\nu} + g_2 \widetilde{F}^{\mu\nu} \right) - iq W_\mu \left[g_1 \, (-J^\mu + \right.$$
$$\left. + \; iq A_\nu F^{\mu\nu}) + iq g_2 A_\nu \widetilde{F}^{\mu\nu} \right] - \xi D_\nu D^\nu D_\mu W^\mu = m^2 D_\nu W^\nu + iq g_1 W_\mu J^\mu - \frac{iq}{2} W_{\mu\nu} F^{\mu\nu} +$$
$$+ \frac{iq}{2} W_{\mu\nu} \left(g_1 F^{\mu\nu} + g_2 \widetilde{F}^{\mu\nu} \right) + g_1 q^2 W_\mu A_\nu F^{\mu\nu} + g_2 q^2 W_\mu A_\nu \widetilde{F}^{\mu\nu} - \xi D_\nu D^\nu D_\mu W^\mu \quad \Rightarrow$$
$$\Rightarrow \quad (m^2 D_\mu + iq g_1 J_\mu) W^\mu + \frac{iq}{2} W_{\mu\nu} [(g_1 - 1) F^{\mu\nu} + g_2 \widetilde{F}^{\mu\nu}] + q^2 W_\mu A_\nu (g_1 F^{\mu\nu} + g_2 \widetilde{F}^{\mu\nu}) -$$
$$- \xi D_\nu D^\nu D_\mu W^\mu = 0 \,.$$

Here the relation $F_{\mu\nu} = -iq^{-1}[D_\mu, D_\nu]$ and the Maxwell equations $\partial_\mu F^{\mu\nu} = J^\nu$ and $\partial_\nu \widetilde{F}^{\mu\nu} = 0$ have been used. The equation ensures that massive vector bosons have three d.o.f.

Noether current for MCPs

According to the Noether's theorem, for every gauge symmetry there is corresponding conserved current,

$$j^\mu = \frac{\partial \mathcal{L}}{\partial(\partial_\mu W_\nu)} \Delta W_\nu + \frac{\partial \mathcal{L}}{\partial(\partial_\mu W_\nu^\dagger)} \Delta W_\nu^\dagger \,,$$

where $\Delta W_\mu = iqW_\mu$ and $\Delta W_\mu^\dagger = -iqW_\mu^\dagger$ are infinitesimal gauge transformations [26, p. 17]. The explicit calculation goes as

$$\frac{\partial \mathcal{L}}{\partial\left(\partial_\mu W_\nu\right)} = -W^{\rho\sigma\dagger}\delta^\mu_\rho\delta^\nu_\sigma + \xi(DW)^\dagger g^{\rho\alpha}\delta^\mu_\rho\delta^\nu_\alpha = -W^{\mu\nu\dagger} + \xi(DW)^\dagger g^{\mu\nu} \,,$$

$$\frac{\partial \mathcal{L}}{\partial\left(\partial_\mu W_\nu^\dagger\right)} = -W^{\rho\sigma}\delta^\mu_\rho\delta^\nu_\sigma + \xi(DW) g^{\rho\alpha}\delta^\mu_\rho\delta^\nu_\alpha = -W^{\mu\nu} + \xi(DW) g^{\mu\nu} \,,$$

from which follows

$$j^\mu = iq\left(W^{\mu\nu}W_\nu^\dagger - W^{\mu\nu\dagger}W_\nu\right) + iq\xi\left[(DW)^\dagger W^\mu - (DW)W^{\mu\dagger}\right] . \tag{A.5}$$

γW^+W^- vertex

The part of the Lagrangian (3.3) contributing to γW^+W^- vertex is

$$\mathcal{L}_{\gamma WW} = iq\{V^{\mu\nu}A_\mu W_\nu^\dagger - V_{\mu\nu}^\dagger A^\mu W^\nu + W_\mu^\dagger W_\nu(g_1 F^{\mu\nu} + g_2\widetilde{F}^{\mu\nu}) + \xi A^\mu[W_\mu(\partial\cdot W^\dagger) - W_\mu^\dagger(\partial\cdot W)]\} \,.$$

The corresponding diagram is depicted in fig. 3.4(a). The following calculation of scattering amplitude is carried out for the process $W^+(j)W^-(k)\gamma(l) \to$ vacuum, meaning that all momenta in fig. 3.4(a) is pointing towards vertex where the particles are annihilated.

$$\begin{aligned}
\mathcal{M} &= i^2 q\varepsilon_\mu(l)\epsilon_\nu^*(k)\left[-ij^\mu\epsilon^\nu(j) + ij^\nu\epsilon^\mu(j)\right] + i^2 q\varepsilon^\mu(l)\epsilon^\nu(j)\left[ik_\mu\epsilon_\nu^*(k) - ik_\nu\epsilon_\mu^*(k)\right] + \\
&+ i^2 q\xi\varepsilon^\mu(l)\left[-ik^\nu\epsilon_\nu^*(k)\epsilon_\mu(j) + ij^\nu\epsilon_\nu(j)\epsilon_\mu^*(k)\right] + i^2 q g_1\epsilon_\mu^*(k)\epsilon_\nu(j)\left[-il^\mu\varepsilon^\nu(l) + il^\nu\varepsilon^\mu(l)\right] + \\
&+ \frac{i^2 q g_2}{2}\epsilon_\mu^*(k)\epsilon_\nu(j)\epsilon^{\mu\nu\rho\sigma}\left[-il_\rho\varepsilon_\sigma(l) + il_\sigma\varepsilon^\rho(l)\right] = -iq\epsilon_\alpha(j)\epsilon_\beta^*(k)\varepsilon_\gamma(l)\times \\
&\times\left[\delta^\gamma_\mu\delta^\beta_\nu\left(j^\nu g^{\mu\alpha} - j^\mu g^{\nu\alpha}\right) + g^{\gamma\mu}g^{\nu\alpha}\left(k_\mu\delta^\beta_\nu - k_\nu\delta^\beta_\mu\right) + i\xi g^{\mu\gamma}\left(j^\nu\delta^\alpha_\nu\delta^\beta_\mu - k^\nu\delta^\beta_\nu\delta^\alpha_\mu\right) + \right. \\
&\left. + g_1\delta^\beta_\mu\delta^\alpha_\nu\left(l^\nu g^{\mu\gamma} - l^\mu g^{\nu\gamma}\right) + \frac{g_2}{2}\delta^\beta_\mu\delta^\alpha_\nu\epsilon^{\mu\nu\rho\sigma}\left(l_\sigma\delta^\rho_\gamma - l_\rho\delta^\sigma_\gamma\right)\right] = -iq\epsilon_\alpha(j)\epsilon_\beta^*(k)\varepsilon_\gamma(l)\times \\
&\times\left[(\xi j + g_1 l - k)^\alpha g^{\beta\gamma} + (j - g_1 l - \xi k)^\beta g^{\alpha\gamma} + (k - j)^\gamma g^{\alpha\beta} - g_2\epsilon^{\alpha\beta\gamma\sigma}l_\sigma\right] .
\end{aligned}$$

Thus the vertex factor reads

$$\mathcal{M}^{\alpha\beta\gamma}(j,k,l) = \quad =$$

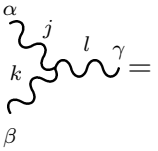

$$= iq\left[(k - g_1 l - \xi j)^\alpha g^{\beta\gamma} + (\xi k + g_1 l - j)^\beta g^{\alpha\gamma} + (j-k)^\gamma g^{\alpha\beta} + g_2 \epsilon^{\alpha\beta\gamma\sigma} l_\sigma\right] . \quad \text{(A.6)}$$

$\gamma\gamma W^+W^-$ vertex

The relevant interaction term for $\gamma\gamma W^+W^-$ vertex is

$$\mathcal{L}_{\gamma\gamma WW} = q^2\left[(\xi+1)A^\mu W_\mu A^\nu W_\nu^\dagger - W^\mu W_\mu^\dagger A^\nu A_\nu\right] ,$$

which produces the graph fig. 3.4(b). Setting the momenta for photons and MCPs as in fig. 5, the scattering amplitude reads

$$\mathcal{M} = iq^2 \varepsilon_\alpha(p_1)\varepsilon_\beta(p_2)\epsilon_\mu(q_-)\epsilon_\nu^*(q_+)\left[(\xi+1)\left(g^{\alpha\mu}g^{\beta\nu} + g^{\beta\mu}g^{\alpha\nu}\right) - 2g^{\mu\nu}g^{\alpha\beta}\right] .$$

This leads to the vertex factor

$$\mathcal{M}^{\alpha\beta\mu\nu} = = iq^2\left[(\xi+1)\left(g^{\alpha\mu}g^{\beta\nu} + g^{\beta\mu}g^{\alpha\nu}\right) - 2g^{\mu\nu}g^{\alpha\beta}\right] . \quad \text{(A.7)}$$

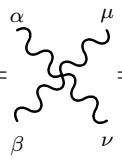

In the adopted conventions, ϵ_α and ε_α correspond to the polarization vectors of a massive vector boson and a photon, respectively; $g^{\mu\nu}$ is the Minkowski metric.

MCP propagator

In order to find the propagator for MCPs one has to first integrate the bilinear part of the Lagrangian:

$$\begin{aligned}
\mathcal{L}_f &= -\frac{1}{2}V_{\mu\nu}^\dagger V^{\mu\nu} + m^2 W_\mu^\dagger W^\mu + \xi\left(\partial_\mu W^\mu\right)\left(\partial^\nu W_\nu^\dagger\right) = \\
&= -\left(\partial^\mu W^\nu\right)\left(\partial_\mu W_\nu^\dagger - \partial_\nu W_\mu^\dagger\right) + m^2 W_\mu^\dagger W^\mu - \xi W^\mu\left(\partial_\mu \partial^\nu W_\nu^\dagger\right) = \\
&= W^\nu\left(\partial^\mu\partial_\mu W_\nu^\dagger - \partial^\mu\partial_\nu W_\mu^\dagger\right) + m^2 W_\mu^\dagger W^\mu - \xi W^\mu\left(\partial_\mu\partial^\nu W_\nu^\dagger\right) = \\
&= W^\nu\left[(\partial^2 + m^2)g_{\mu\nu} - (\xi+1)\partial_\mu\partial_\nu\right] W^{\mu\dagger} .
\end{aligned}$$

The bilinear term in momentum space reads

$$\widetilde{D}^F_{\mu\nu}(k) = -\left(k^2 - m^2\right) g_{\mu\nu} + (\xi + 1) k_\mu k_\nu \,,$$

the inverse of which is the propagator $D^F_{\mu\nu}(k)$. It must be symmetric in its indices because it is impossible to construct an anti-symmetric rank-2 tensor with only one vector. Therefore, the propagator has the form $D^F_{\mu\nu}(k) = A(k^2) g_{\mu\nu} + B(k^2) k_\mu k_\nu$, the coefficients of which can be found by imposing $D^{F\mu\nu}(k)\widetilde{D}^F_{\nu\rho}(k) = \delta^\mu_\rho$:

$$\begin{aligned}
\delta^\mu_\rho &= (A g^{\mu\nu} + B k^\mu k^\nu)\left[(m^2 - k^2) g_{\nu\rho} + (\xi + 1) k_\nu k_\rho\right] = \\
&= A(m^2 - k^2)\delta^\mu_\rho + A(\xi + 1) k^\mu k_\rho + B(m^2 - k^2) k^\mu k_\rho + B(\xi + 1) k^2 k^\mu k_\rho = \\
&= A\left[-(k^2 - m^2)\right]\delta^\mu_\rho + k^\mu k_\rho \left[A(\xi + 1) + B(\xi k^2 + m^2)\right] \,.
\end{aligned}$$

By choosing $A = -\frac{1}{k^2 - m^2}$ it follows that

$$A(\xi + 1) + B(\xi k^2 + m^2) = 0 \quad \Rightarrow \quad B = -\frac{A(\xi + 1)}{\xi k^2 + m^2} = \frac{\xi + 1}{(k^2 - m^2)(\xi k^2 + m^2)} \,.$$

Noticing that

$$\frac{\xi + 1}{\xi k^2 + m^2} - \frac{1}{m^2} = \frac{m^2(\xi + 1) - \xi k^2 - m^2}{m^2(\xi k^2 + m^2)} = -\frac{\xi(k^2 - m^2)}{m^2(\xi k^2 + m^2)} \,,$$

the propagator can be written as

$$D^F_{\mu\nu}(k) = \frac{-g_{\mu\nu} + k_\mu k_\nu / m^2}{k^2 - m^2} - \frac{\xi k_\mu k_\nu}{m^2(\xi k^2 + m^2)} \equiv \frac{P_{\mu\nu}(k)}{k^2 - m^2} - \frac{k_\mu k_\nu}{m^2} \cdot \frac{\xi}{\xi k^2 + m^2} \,.$$

Magnetic moment in MCP Lagrangian

In order to show that the minimal substitution generates coupling between spin and magnetic field in non-relativistic approximation, one needs to integrate the relevant piece of the Lagrangian by parts,

$$\begin{aligned}
\mathcal{L}_{\text{mc,g}} &= iq(V^{\mu\nu} A_\mu W^\dagger_\nu - V^\dagger_{\mu\nu} A^\mu W^\nu) = \\
&= iq[F^{\mu\nu} W^\dagger_\mu W_\nu + (\partial \cdot W^\dagger)(W \cdot A) - (\partial \cdot W)(W^\dagger \cdot A) + A^\mu (W^{\nu\dagger} \partial_\mu W_\nu - W^\nu \partial_\mu W^\dagger_\nu)] \,,
\end{aligned}$$

where the following relations have been used:

$$
\begin{aligned}
V^{\mu\nu}A_\mu W^\dagger_\nu &= (\partial^\mu W^\nu - \partial^\nu W^\mu)A_\mu W^\dagger_\nu = \\
&= [\partial^\mu(W^\nu A_\mu W^\dagger_\nu) = (\partial^\mu W^\nu)A_\mu W^\dagger_\nu + (\partial\cdot A)(W^\dagger\cdot W) + (\partial^\mu W^{\nu\dagger})A_\mu W_\nu \simeq 0\,, \\
&\quad\ \partial^\nu(W^\mu A_\mu W^\dagger_\nu) = (\partial^\nu W^\mu)A_\mu W^\dagger_\nu + (\partial\cdot W^\dagger)(W\cdot A) + (\partial^\nu A^\mu)W_\mu W^\dagger_\nu \simeq 0] = \\
&= (\partial\cdot W^\dagger)(W\cdot A) + (\partial^\nu A^\mu)W_\mu W^\dagger_\nu - (\partial\cdot A)(W^\dagger\cdot W) - (\partial^\mu W^{\nu\dagger})A_\mu W_\nu\,,
\end{aligned}
$$

$$
\begin{aligned}
V^\dagger_{\mu\nu}A^\mu W^\nu &= (\partial_\mu W^\dagger_\nu - \partial_\nu W^\dagger_\mu)A^\mu W^\nu = \\
&= [\partial_\mu(W^\dagger_\nu A^\mu W^\nu) = (\partial_\mu W^\dagger_\nu)A^\mu W^\nu + (\partial\cdot A)(W^\dagger\cdot W) + (\partial_\mu W_\nu)W^{\nu\dagger}A^\mu \simeq 0\,, \\
&\quad\ \partial_\nu(W^\dagger_\mu A^\mu W^\nu) = (\partial_\nu W^\dagger_\mu)A^\mu W^\nu + (\partial\cdot W)(W^\dagger\cdot A) + (\partial_\nu A_\mu)W^{\mu\dagger}W^\nu \simeq 0] = \\
&= (\partial\cdot W)(W^\dagger\cdot A) + (\partial_\nu A_\mu)W^{\mu\dagger}W^\nu - (\partial\cdot A)(W^\dagger\cdot W) - (\partial_\mu W_\nu)W^{\nu\dagger}A^\mu\,.
\end{aligned}
$$

A.1.2. Polarization projectors

Assuming the axis of collision is the z-axis, the left- and right-handed polarization vectors in normal basis are $\varepsilon^-_\mu = \frac{1}{\sqrt{2}}(0\ 1\ -i\ 0)^T$ and $\varepsilon^+_\mu = \frac{1}{\sqrt{2}}(0\ 1\ i\ 0)^T$, respectively. The corresponding projection tensors are

$$
P^-_{\mu\nu} = \varepsilon^-_\mu\varepsilon^{-*}_\nu = \frac{1}{2}\begin{pmatrix} 0 & 0 & 0 & 0 \\ 0 & 1 & i & 0 \\ 0 & -i & 1 & 0 \\ 0 & 0 & 0 & 0 \end{pmatrix} \quad \text{and} \quad P^+_{\mu\nu} = \varepsilon^+_\mu\varepsilon^{+*}_\nu = \frac{1}{2}\begin{pmatrix} 0 & 0 & 0 & 0 \\ 0 & 1 & -i & 0 \\ 0 & i & 1 & 0 \\ 0 & 0 & 0 & 0 \end{pmatrix}. \tag{A.8}
$$

Let the incoming photons in c.m. have 4-momenta $q^\mu = (q^0\ 0\ 0\ q^0)^T$ and $p^\mu = (p^0\ 0\ 0\ p^0)^T$, and let the particle associated with momentum q^μ be traveling towards z-axis. Since $\mathbf{q} = -\mathbf{p}$ in c.m. frame it must be the case that $q^\mu = (p^0\ 0\ 0\ -p^0)^T$ and $p^\mu = (q^0\ 0\ 0\ -q^0)^T$ due to the photon dispersion relation. Noticing that

$$
q^\mu p^\nu + p^\mu q^\nu = q\cdot p\begin{pmatrix} 1 & 0 & 0 & 0 \\ 0 & 0 & 0 & 0 \\ 0 & 0 & 0 & 0 \\ 0 & 0 & 0 & 1 \end{pmatrix},
$$

the projection into the space spanned by transversal polarization vectors can be written as

$$
P^{\mu\nu}(q,\,p) = \frac{q^\mu p^\nu + p^\mu q^\nu}{q\cdot p} - g^{\mu\nu} = \begin{pmatrix} 0 & 0 & 0 & 0 \\ 0 & 1 & 0 & 0 \\ 0 & 0 & 1 & 0 \\ 0 & 0 & 0 & 0 \end{pmatrix}.
$$

The off-diagonal terms in (A.8) can be generated with

$$
i\epsilon^{\mu\nu\rho\sigma}q_\rho p_\sigma = q\cdot p\begin{pmatrix} 0 & 0 & 0 & 0 \\ 0 & 0 & -i & 0 \\ 0 & i & 0 & 0 \\ 0 & 0 & 0 & 0 \end{pmatrix}
$$

which after normalization leads to the definition of $F_{\mu\nu}(q,\,p)$ in (3.13). After pulling things together it is easy to see that

$$P^{\pm}_{\mu\nu}(q,\,p) = \frac{1}{2}\left[P_{\mu\nu}(q,\,p) \pm F_{\mu\nu}(q,\,p)\right] = \frac{q^\mu p^\nu + p^\mu q^\nu \pm i\epsilon_{\mu\nu\rho\sigma}q^\rho p^\sigma}{q\cdot p} - g^{\mu\nu} = \frac{1}{2}\begin{pmatrix} 0 & 0 & 0 & 0 \\ 0 & 1 & \mp i & 0 \\ 0 & \pm i & 1 & 0 \\ 0 & 0 & 0 & 0 \end{pmatrix}.$$

Although the result was derived for particular axis of collision and for normal basis of vector space, it holds for any frame of reference. Also, the following properties were previously used:

$$\begin{gathered} P^{\mu\nu}(q,\,p) = P^{\mu\nu}(p,\,q)\,, \\ P^{\mu\nu}(q+p,\,q) = \tfrac{(q+p)^\mu q^\nu + q^\mu (q+p)^\nu}{(q+p)\cdot q} - g^{\mu\nu} = P^{\mu\nu}(p,\,q) + \tfrac{q^\mu q^\nu + q^\nu p^\mu}{q\cdot p}\,, \\ F^{\mu\nu}(q+p,\,p) = F^{\mu\nu}(q,\,p) = -F^{\mu\nu}(p,\,q) = -F^{\mu\nu}(q+p,\,q)\,. \end{gathered}$$

A.1.3. Polarized cross-sections and asymmetries

If the polarized cross-section is given by $\mathrm{d}\sigma_{r_1 r_2} = \mathrm{d}\left(\sigma + r_1\sigma_1 + r_2\sigma_2 + r_{12}\sigma_{12}\right)$, where r_1 and r_2 are the helicity states of the first and the second initial photon, respectively, and

$$\begin{array}{llll} \mathrm{d}\sigma &= \frac{1}{4}\frac{\mathrm{d}t\;\Theta(s-4m^2)}{16\pi s^2}\,\mathcal{A}^{\alpha\beta\alpha'\beta'}g_{\alpha\alpha'}g_{\beta\beta'} & \mathrm{d}\sigma_1 &= \frac{1}{4}\frac{\mathrm{d}t\;\Theta(s-4m^2)}{16\pi s^2}\,\mathcal{A}^{\alpha\beta\alpha'\beta'}F_{\alpha\alpha'}g_{\beta\beta'}, \\ \mathrm{d}\sigma_2 &= -\frac{1}{4}\frac{\mathrm{d}t\;\Theta(s-4m^2)}{16\pi s^2}\,\mathcal{A}^{\alpha\beta\alpha'\beta'}g_{\alpha\alpha'}F_{\beta\beta'}, & \mathrm{d}\sigma_{12} &= -\frac{1}{4}\frac{\mathrm{d}t\;\Theta(s-4m^2)}{16\pi s^2}\,\mathcal{A}^{\alpha\beta\alpha'\beta'}F_{\alpha\alpha'}F_{\beta\beta'}, \end{array} \tag{A.9}$$

then all four polarized cross-sections in terms of asymmetry cross-sections are

$$\begin{aligned} \mathrm{d}\sigma_{++} &= \mathrm{d}\left(\sigma + \sigma_1 + \sigma_2 + \sigma_{12}\right), & \mathrm{d}\sigma_{+-} &= \mathrm{d}\left(\sigma + \sigma_1 - \sigma_2 - \sigma_{12}\right), \\ \mathrm{d}\sigma_{-+} &= \mathrm{d}\left(\sigma - \sigma_1 + \sigma_2 - \sigma_{12}\right), & \mathrm{d}\sigma_{--} &= \mathrm{d}\left(\sigma - \sigma_1 - \sigma_2 + \sigma_{12}\right), \end{aligned}$$

and the asymmetry cross-sections in terms of polarized cross-sections

$$\begin{aligned} \mathrm{d}\sigma &= \tfrac{1}{4}\,\mathrm{d}\left(\sigma_{++} + \sigma_{+-} + \sigma_{-+} + \sigma_{--}\right), & \mathrm{d}\sigma_1 &= \tfrac{1}{4}\,\mathrm{d}\left(\sigma_{++} + \sigma_{+-} - \sigma_{-+} - \sigma_{--}\right), \\ \mathrm{d}\sigma_2 &= \tfrac{1}{4}\,\mathrm{d}\left(\sigma_{++} - \sigma_{+-} + \sigma_{-+} - \sigma_{--}\right), & \mathrm{d}\sigma_{12} &= \tfrac{1}{4}\,\mathrm{d}\left(\sigma_{++} - \sigma_{+-} - \sigma_{-+} + \sigma_{--}\right). \end{aligned}$$

A.2. Scalar and fermion case

A.2.1. Feynman diagrams and rules

Scalar case $\gamma\gamma \to \phi^+\phi^-$

The Lagrangian for scalar particles invariant under local $U(1)$ transformations reads

$$\begin{aligned} \mathcal{L} &= |D\phi|^2 - m^2\,|\phi|^2 - \frac{1}{4}F^2 = \\ &= |\partial\phi|^2 - m^2\,|\phi|^2 + iqA\left(\phi^\dagger\partial\phi - \phi\partial\phi^\dagger\right) + q^2A^2\,|\phi|^2 - \frac{1}{4}F^2\,, \end{aligned} \tag{A.10}$$

which produces the following rules (c.f. scalar QED rules in [29, p. 801]), with all momenta incoming:

$|\partial\phi|^2 - m^2|\phi|^2 \quad \Rightarrow$ 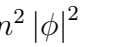 $= \frac{i}{p^2-m^2}$ scalar MCP propagator,

$iqA\left(\phi^\dagger\partial\phi - \phi\partial\phi^\dagger\right) \quad \Rightarrow$ 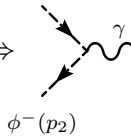 $= iq(p_1-p_2)_\mu$ MCP-photon vertex,

$q^2A^2|\phi|^2 \quad \Rightarrow$ 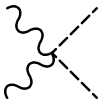 $= 2iq^2g^{\mu\nu}$ photon-MCP vertex.

All possible Feynman diagrams for the process $\gamma\gamma \to \phi^+\phi^-$ are depicted in fig. 15.

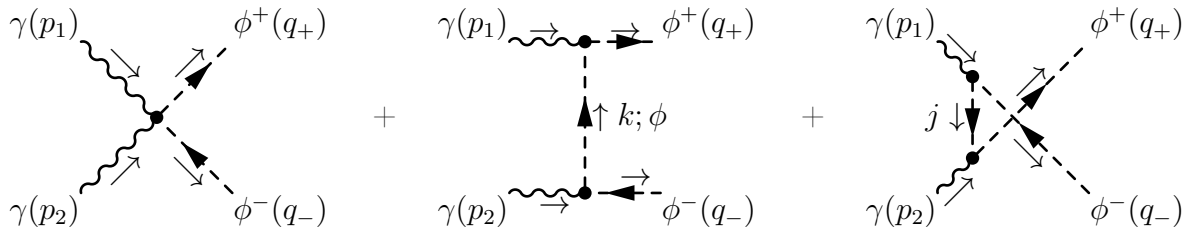

Figure 15: Leading order contributions of the process $\gamma\gamma \to \phi^+\phi^-$.

The amplitude for the process is given by

$$\begin{aligned}\mathcal{M}_0 = 2iq^2g^{\mu\nu}\varepsilon_\mu^{r_1}(p_1)\varepsilon_\nu^{r_2}(p_2) + \varepsilon_\mu^{r_1}(p_1)\varepsilon_\nu^{r_2}(p_2)iq(-q_+-k)^\mu\frac{i}{k^2-m^2}iq(-k+q_-)^\nu + \\ + \varepsilon_\mu^{r_1}(p_1)\varepsilon_\nu^{r_2}(p_2)iq(-j+q_-)^\mu\frac{i}{j^2-m^2}iq(-q_+-j)^\nu = iq^2\varepsilon_\mu^{r_1}(p_1)\varepsilon_\nu^{r_2}(p_2)\mathcal{M}_0^{\mu\nu},\end{aligned} \tag{A.11}$$

where

$$\mathcal{M}_0^{\mu\nu} = 2g^{\mu\nu} + \frac{(q_++k)^\mu(q_--k)^\nu}{t-m^2} + \frac{(q_--j)^\mu(q_++j)^\nu}{u-m^2} \tag{A.12}$$

and

$$t = k^2 = (q_+-p_1)^2 = (p_2-q_-)^2, \quad u = j^2 = (q_+-p_2)^2 = (p_1-q_-)^2. \tag{A.13}$$

Fermion case $\gamma\gamma \to f^+f^-$

The suitable Lagrangian for $\gamma\gamma \to f^+f^-$ is the QED one with the replacement of electron charge with millicharge, $e \to q$. The Feynman rules for corresponding amplitude of the

diagrams in fig. 16 are

$-q\bar{\psi}\gamma^\mu\psi A_\mu \quad \Rightarrow$ 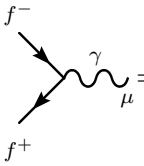 $= -iq\gamma^\mu$ electron-photon vertex,

$\bar{\psi}(i\partial\!\!\!/ - m)\psi \quad \Rightarrow$ $= \frac{i}{\not{p}-m}$ fermion MCP propagator.

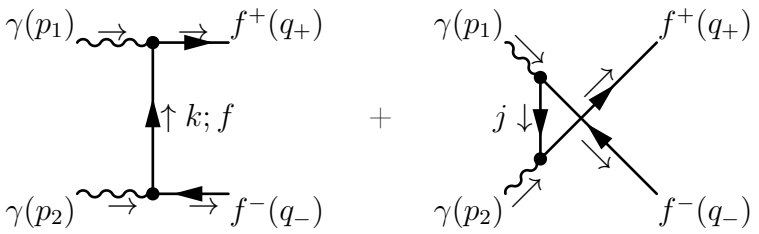

Figure 16: Leading order contributions of the process $\gamma\gamma \to f^+f^-$.

The amplitude reads

$$\mathcal{M}_{1/2} = \varepsilon_\mu^{r_1}(p_1)\varepsilon_\nu^{r_1}(p_2)\bar{u}^s(q_+)\left[(-iq\gamma^\mu)\frac{i}{\not{k}-m}(-iq\gamma^\nu) + (-iq\gamma^\nu)\frac{i}{\not{j}-m}(-iq\gamma^\mu)\right]v^{s'}(q_-) =$$
$$= iq^2\varepsilon_\mu^{r_1}(p_1)\varepsilon_\nu^{r_1}(p_2)\bar{u}^s(q_+)\mathcal{M}_{1/2}^{\mu\nu}v^{s'}(q_-)\,, \tag{A.14}$$

where j and k are given by (A.13) and

$$\mathcal{M}_{1/2}^{\mu\nu} = \frac{\gamma^\mu\gamma^\nu}{\not{k}-m} + \frac{\gamma^\nu\gamma^\nu}{\not{j}-m}\,.$$

A.2.2. Cross-section

The calculation of polarized cross-sections for scalar boson and fermion MCPs is the same as in section 3.3 and appendix A.1, with the only difference being the squared amplitude summed over final states,

$$\mathcal{A} = \sum_{\text{final states}} |\mathcal{M}|^2\,.$$

The cross-section asymmetries are still given by (A.9).

Scalar case

In the scalar case, the squared amplitude simply reads

$$\mathcal{A}_0^{\alpha\beta\alpha'\beta'} = \mathcal{M}_0^{\alpha\beta}\mathcal{M}_0^{*\alpha'\beta'}\,.$$

Since there's no parity violation in the theory, the asymmetry cross-sections are zero: $\sigma_1^{(0)} = \sigma_2^{(0)} = 0$. The FeynCalc package gives the following averaged cross-section, $\bar{\sigma}^{(0)}$, and asymmetry cross-section, $\sigma_{12}^{(0)}$:

$$\bar{\sigma}^{(0)}(\beta) = \frac{\bar{\sigma}_\infty}{16}(1-\beta^2)\left[\beta(2-\beta^2) + (\beta^4-1)\,\mathrm{atanh}\,\beta\right]\,, \tag{A.15}$$

$$\sigma_{12}^{(0)}(\beta) = \frac{\bar{\sigma}_\infty}{16}(1-\beta^2)\left[\beta + (1-\beta^2)\ln\left(\frac{2}{1+\beta}-1\right)\right]\,, \tag{A.16}$$

where $\bar{\sigma}_\infty = \frac{q^4}{2\pi m^2}$ is the asymptotic cross-section for vector MCPs of the same process. It is easy to see by inspection that, unlike in the vector boson case, the averaged cross-section for $\gamma\gamma \to$ scalar MCPs goes asymptotically to zero as the c.m. energy increases.

Fermion case

The squared amplitude here can be written as

$$\mathcal{A}_{1/2}^{\mu\nu\mu'\nu'} = \sum_{s,s'} \bar{u}^s(q_+)\mathcal{M}_{1/2}^{\mu\nu}v^{s'}(q_-)\left[\bar{u}^s(q_+)\mathcal{M}_{1/2}^{\mu'\nu'}v^{s'}(q_-)\right]^*\,,$$

where the sum runs over spinor states s and s'. Since $(\gamma^0)^2 = 1$ and $\gamma^{\mu\dagger} = \gamma^0\gamma^\mu\gamma^0$, it follows that

$$(\bar{u}\gamma^\mu\gamma^\nu v)^* = (u^\dagger\gamma^0\gamma^\mu\gamma^\nu v)^* = v^\dagger\gamma^{\nu\dagger}\gamma^{\mu\dagger}\gamma^{0\dagger}u = v^\dagger\gamma^0\gamma^\nu\gamma^0\gamma^0\gamma^\nu\gamma^0\gamma^0 u = \bar{v}\gamma^\nu\gamma^\mu u\,.$$

Analogous to the polarization vectors, there's also a completeness relation for fermions as well:

$$\sum_s u^s(p)\bar{u}^s(p) = \not{p} + m\,, \quad \sum_s v^s(p)\bar{v}^s(p) = \not{p} - m\,.$$

The above enables to write the squared amplitude as follows:

$$\begin{aligned}\mathcal{A}_{1/2}^{\mu\nu\mu'\nu'} &= \sum_{s,s'} \bar{u}^s(q_+)\mathcal{M}_{1/2}^{\mu\nu}v^{s'}(q_-)\left[\bar{u}^s(q_+)\mathcal{M}_{1/2}^{\mu\nu}v^{s'}(q_-)\right]^* = \\ &= \sum_{s,s'} \bar{u}^s(q_+)\mathcal{M}_{1/2}^{\mu\nu}v^{s'}(q_-)\bar{v}^{s'}(q_-)\mathcal{M}_{1/2}^{\nu'\mu'}u^s(q_+) = \\ &= \sum_s \bar{u}^s(q_+)\mathcal{M}_{1/2}^{\mu\nu}(\not{q}_- - m)\mathcal{M}_{1/2}^{\nu'\mu'}u^s(q_+)\,.\end{aligned}$$

The last line can be further simplified by writing it in spinor and matrix indices (the summation over which is implied):

$$\begin{aligned}
\mathcal{A}_{1/2}^{\mu\nu\mu'\nu'} &= \sum_s \bar{u}^s(q_+)\mathcal{M}_{1/2}^{\mu\nu}(\not{q}_- - m)\mathcal{M}_{1/2}^{\nu'\mu'}u^s(q_+) = \\
&= \sum_s \bar{u}^s(q_+)_a \left(\mathcal{M}_{1/2}^{\mu\nu}\right)_{ab}(\not{q}_- - m)_{bc}\left(\mathcal{M}_{1/2}^{\nu'\mu'}\right)_{cd} u^s(q_+)_d = \\
&= \left(\mathcal{M}_{1/2}^{\mu\nu}\right)_{ab}(\not{q}_- - m)_{bc}\left(\mathcal{M}_{1/2}^{\nu'\mu'}\right)_{cd}\sum_s u^s(q_+)_d\bar{u}^s(q_+)_a = \\
&= \left(\mathcal{M}_{1/2}^{\mu\nu}\right)_{ab}(\not{q}_- - m)_{bc}\left(\mathcal{M}_{1/2}^{\nu'\mu'}\right)_{cd}(\not{q}_+ + m)_{da} = \\
&= \mathrm{Tr}\left[\mathcal{M}_{1/2}^{\mu\nu}(\not{q}_- - m)\mathcal{M}_{1/2}^{\nu'\mu'}(\not{q}_+ + m)\right] .
\end{aligned}$$

Plugging the amplitude into (A.9) results in the following averaged cross-section, $\bar{\sigma}^{(1/2)}$, and asymmetry cross-section, $\sigma_{12}^{(1/2)}$:

$$\bar{\sigma}^{(1/2)}(\beta) = \frac{\bar{\sigma}_\infty}{8}(\beta^2-1)\left[\beta(2-\beta^2) + (\beta^4-3)\,\mathrm{atanh}\,\beta\right] , \tag{A.17}$$

$$\sigma_{12}^{(1/2)}(\beta) = \frac{\bar{\sigma}_\infty}{8}(\beta^2-1)\left(3\beta - 2\,\mathrm{atanh}\,\beta\right) . \tag{A.18}$$

B. Boltzmann equation

B.1. Definitions

- n-th modified Bessel function of the second kind:

$$K_n(x) = \frac{\sqrt{\pi}}{\Gamma\left(n+\frac{1}{2}\right)}\left(\frac{x}{2}\right)^n \int_1^\infty e^{-zx}(z^2-1)^{n-\frac{1}{2}}\,\mathrm{d}z\,. \tag{B.1}$$

B.2. Simplifications

- From (4.1) to (4.3), the following transformations are needed:

$$\frac{\mathrm{d}Y}{\mathrm{d}t} = \frac{\dot{n}}{n_\gamma} - \frac{n}{n_\gamma^2}\dot{n}_\gamma = \frac{\dot{n}}{n_\gamma} - \frac{n}{n_\gamma^2}\cdot\frac{2\zeta(3)\cdot 3T^2}{\pi^2}\cdot\frac{\mathrm{d}T}{\mathrm{d}t} = \frac{\dot{n}}{n_\gamma} + 3H\frac{n}{n_\gamma}\,,$$

$$\frac{\mathrm{d}}{\mathrm{d}t} = \frac{\mathrm{d}x}{\mathrm{d}t}\frac{\mathrm{d}}{\mathrm{d}x} = -\frac{m}{T^2}\frac{\mathrm{d}T}{\mathrm{d}t}\cdot\frac{\mathrm{d}}{\mathrm{d}x} = \frac{mH}{T}\frac{\mathrm{d}}{\mathrm{d}x} = xH\frac{\mathrm{d}}{\mathrm{d}x}\,.$$

- Equilibrium number density accounting different energy distributions for fermions ($\eta = 1$) and bosons ($\eta = -1$):

$$\begin{aligned}
n_{EQ}^{(\eta)} &= \frac{g}{(2\pi)^2}\int \mathrm{d}^3\mathbf{p} f^{EQ} = \frac{g}{(2\pi)^2}\cdot 4\pi\int_0^\infty \frac{|\mathbf{p}|^2\,\mathrm{d}\,|\mathbf{p}|}{e^{\frac{E}{T}}+\eta} = \frac{g}{2\pi^2}\int_m^\infty \frac{\sqrt{E^2-m^2}E\,\mathrm{d}E}{e^{\frac{E}{T}}+\eta} = \\
&= \frac{g}{2\pi^2}m^3\int_m^\infty \frac{\sqrt{\frac{E}{m}-1}\frac{E}{m}\,\mathrm{d}\left(\frac{E}{m}\right)}{e^{\frac{E}{m}\cdot\frac{m}{T}}+\eta} = \frac{g}{2\pi^2}m^3\int_1^\infty \frac{z\sqrt{z^2-1}\,\mathrm{d}z}{e^{zx}+\eta} = \\
&= \left[\frac{1}{e^{zx}+\eta} = \sum_{n=1}^\infty e^{-nzx}(-\eta)^{n-1}\right] = \frac{g}{2\pi^2}m^3\sum_{n=1}^\infty(-\eta)^{n-1}\int_1^\infty e^{-nxz}z\sqrt{z^2-1}\,\mathrm{d}z = \\
&= \left[\frac{\mathrm{d}}{\mathrm{d}z}\left[e^{-nxz}\left(\sqrt{y^2-1}\right)^3\right] = -nxe^{-nxz}\left(z^2-1\right)^{\frac{3}{2}} + 3e^{-nxz}\sqrt{z^2-1}z\right] = \\
&= \frac{g}{2\pi^2}\cdot\frac{m^3}{3}\sum_{n=1}^\infty(-\eta)^{n-1}\Big[\underbrace{e^{-nxz}\left(z^2-1\right)^{\frac{3}{2}}\Big|_1^\infty}_{=0} + n\int_1^\infty xe^{-nxz}\left(z^2-1\right)^{\frac{1}{2}}\mathrm{d}z\Big] = \\
&= \frac{g}{2\pi^2}m^3\sum_{n=1}^\infty(-\eta)^{n-1}\frac{nx}{3}\int_1^\infty e^{-nxz}\sqrt{z^2-1}\,\mathrm{d}z = \left[K_2(x) = \frac{x^2}{3}\int_1^\infty e^{-zx}\sqrt{z^2-1}\,\mathrm{d}z\right] = \\
&= \frac{g}{2\pi^2}m^3\sum_{n=1}^\infty\frac{K_2(nx)}{nx}(-\eta)^{n-1} = \frac{g}{2\pi^2}m^2T\sum_{n=1}^\infty\frac{K_2(nx)}{n}(-\eta)^{n-1} = \\
&= \frac{g}{2\pi^2}x^2T^3\sum_{n=1}^\infty\frac{K_2(nx)}{n}(-\eta)^{n-1}\,.
\end{aligned}$$